

TABLE OF CONTENTS

The Ferromagnetic Phase in Silmanal and Related Alloys

LIST OF TABLES 10

LIST OF FIGURES 11

ACKNOWLEDGMENTS 12

ABSTRACT 13

1. INTRODUCTION 14

2. EXPERIMENTAL 15

2.1 Materials 15

2.2 Preparation 16

2.3 Characterization 17

2.4 X-ray Investigation 18

2.5 Magnetic Measurements 19

2.6 Electron Microscopy 20

2.7 Differential Thermal Analysis (DTA) 21

by

H. A. KAZI, M.E.

A Thesis Submitted to the
Faculty of Graduate Studies in
Partial Fulfillment of the Requirements
for the Degree of
Doctor of Philosophy
Major Subject: Metallurgical Engineering

Approved

C. H. Castelly
.....

M. R. Joran
.....

H. V. Gow
.....

.....

TABLE OF CONTENTS

LIST OF TABLES	iv
LIST OF FIGURES	vi
ACKNOWLEDGEMENTS	ix
ABSTRACT	x
1. INTRODUCTION	1
2. EXPERIMENTAL	
2.1 Materials	9
2.2 Preparation of Samples	9
2.3 Chemical Analysis	12
2.4 X-ray Investigation	12
2.5 Magnetic Measurements	14
2.6 Hardness Measurements	19
2.7 Metallographic Examination	19
2.8 Electron Microscopy	20
2.9 Differential Thermal Analysis (DTA)	22
3. RESULTS AND DISCUSSION	
3.1 Phase Relations in the Binary Mn-Al System around the Composition of MnAl	23
3.2 Phase Relations in Silmanal	26
3.3 Magnetic Properties of Silmanal	45
3.4 The τ -Phase in Alloys with Small Ag Content	48

3.5	The Effect of Small Additions of Cu and Ni	55
3.6	Replacement of Al in Silmanal by Sb	56
4.	SUMMARY AND CONCLUSIONS	59
	REFERENCES	110

	γ -phase given by Runt (31)	67
Table 1	β -phase of Table 2 compared with that of A.3.7.7.4.1	68
	Card No. 11-215	68
Table 2	β - β' phase of Table 2 compared with that of A.3.7.7.4.1	69
	Card No. 1-1871	69
Table 3	X-ray analysis of Silmanal powder	70
Table 4a	X-ray analysis of Silmanal strip sheet 115 mm long	71
Table 5	Relative abundance of precipitated phases in Silmanal aged at various temperatures	72
Table 6	Relative amount of β and β' phases in Silmanal aged at different temperatures	73
Table 7	Identification and interplanar distance of wire aged at 260°C and aged in 20% ammonia solution	74
Table 8	Identification and interplanar distance of precipitates observed in Silmanal sheet in 20%	75

LIST OF TABLES

Table 1	Phase relations, magnetic and mechanical conditions of $Mn_{1+X}Al$ alloys	65
Table 2	X-ray analysis of $Mn_{1.25}Al$ alloy	66
Table 3	τ -Phase of Table 2 compared with that of the τ -phase given by Kono (31)	67
Table 4	h -Phase of Table 2 compared with that of A.S.T.M. Card No. 11-416	68
Table 5	β -Mn phase of Table 2 compared with that of A.S.T.M. Card No. 1-1234	69
Table 6	X-ray analysis of Silmanal powder	70
Table 6a	X-ray analysis of Silmanal strip etched in mercury ...	71
Table 7	Relative abundance of precipitated phases in Silmanal aged at various temperatures	72
Table 8	Lattice constant of Ag and Ag-mixed crystal in Silmanal aged at different temperatures	73
Table 9	Intensities and interplanar distances of a Silmanal wire aged at 240°C and etched in KCN- ammoniumpersulphate	74
Table 10	Intensities and interplanar distances of precipitated phases observed in Silmanal etched in mercury	75

Table 11	Rockwell hardness of Silmanal aged at various temperatures	76
Table 12	I_s , I_r and I_c of Silmanal after various heat treatments	77
Table 13	Phase relations in $Ag_xMn_{1.11}Al_{0.89}$ with $X = 0.02, 0.1, 0.2$ and 2	78
Table 14	I_s , I_r and I_c of Ag-Al-Mn alloys other than Silmanal, and of Ag_5MnSb	80
Table 15	Curie temperatures of Silmanal and related alloys	81

LIST OF FIGURES

Figure 1	Bethe's curve	82
Figure 2	Isomagnetization curve of Silmanal	83
Figure 3a	Photograph: Holder for samples and pick-up coil	84
Figure 3b	Photograph: Setup for magnetic measurements	85
Figure 4a	Photograph: Sample holder for Curie point measurements	86
Figure 4b	Photograph: Apparatus for Curie temperature measurements	87
Figure 5	Photograph: Diffractometer charts for Silmanal sheets aged at different temperatures	88
Figure 6a	Photograph: X-ray film from Silmanal strip sample aged at 240°C	89
Figure 6b	Photograph: X-ray film from Silmanal strip sample aged at 240°C and etched in mercury	89
Figure 7	Photograph: Diffraction chart of Silmanal sheet sample before and after etching	90
Figure 8	Graph: Differential thermal curve	91
Figure 9	Graph: Rockwell hardness of Silmanal vs. temperature	92
Figure 10a	Micrograph: Microstructure of quenched Silmanal ...	93
Figure 10b	Micrograph: Microstructure of Silmanal aged at 240°C	93

Figure 10c	Micrograph: EM300: Carbon replica of Silmanal sample aged at 240°C	94
Figure 10d	Micrograph: EM300: Transmission micrograph of Silmanal sample aged at 240°C	95
Figure 10e	Micrograph: Microstructure of Silmanal aged at 400°C	96
Figure 11	Graph: Hysteresis loop of Silmanal aged for 168 hours at 240°C	97
Figure 12	Graph: Hysteresis loop of Silmanal aged for 76 hours at 240°C in a magnetic field	98
Figure 13	Graph: Hysteresis loop of Silmanal aged for 500 hours at 200°C	99
Figure 14	Graph: Hysteresis loop of Silmanal aged for 168 hours at 200°C	100
Figure 15	Graph: Saturation magnetization of Silmanal vs. aging time	101
Figure 16a	Micrograph: Microstructure of $Mn_{1.11}Al_{0.89}$ aged at 300°C	102
Figure 16b	Micrograph: Microstructure of $Ag_{0.1}Mn_{1.11}Al_{0.89}$ aged at 300°C	102
Figure 16c	Micrograph: Microstructure of $Ag_{0.2}Mn_{1.11}Al_{0.89}$ aged at 300°C	103
Figure 16d	Micrograph: EM300: Magnetic colloid replica of $Ag_{0.2}Mn_{1.11}Al_{0.89}$ aged at 300°C	103

Figure 17a	Electron probe micrograph of $\text{Ag}_{0.2}\text{Mn}_{1.11}\text{Al}_{0.89}$	104
Figure 17b	Electron probe micrograph: current image with superimposed X-ray scan	104
Figure 17c	Electron probe micrograph: current image with superimposed X-ray scan	105
Figure 18a	Graph: Hysteresis loop of cast $\text{Ag}_{0.2}\text{Mn}_{1.11}\text{Al}_{0.89}$	106
Figure 18b	Graph: Hysteresis loop of cast $\text{Ag}_{0.2}\text{Mn}_{1.11}\text{Al}_{0.89}$ aged for 100 hours at 300°C	106
Figure 19	Graph: Hysteresis loop of Ag_2MnAl aged for 168 hours at 240°C	107
Figure 20a	Micrograph: Microstructure of unetched Ag_5MnSb	108
Figure 20b	Micrograph: Magnetic colloid on Ag_5MnSb	108
Figure 21	Graph: Hysteresis loop of Ag_5MnSb aged for 200 hours at 140°C	109

ACKNOWLEDGEMENTS

The author wishes to express his appreciation to Dr. L. M. Castelliz for her constant interest and guidance which she offered during the course of the work. The author also acknowledges the valuable assistance provided by Dr. K. V. Gow and Dean M. R. Foran. In addition, help afforded by Mssrs. Zia-ul-Haq and P. Boucher is much appreciated.

The project was made possible by a grant to Dr. L. M. Castelliz from the National Research Council, Ottawa, Canada.

ABSTRACT

The subject of this research program was the kinetic relations in various composition fields of the ternary system Ag-Mn-Al over a range of temperatures. The purpose of this study was to identify the ferromagnetic constituent and the source of the high coercive force in Silmanal. The rôle of Ag in the reaction kinetics and stabilization of the ferromagnetic phase in Silmanal was traced by comparative study of phase relations in binary Mn-Al alloys and alloys with small additions of Cu or Ni to MnAl. The effect of replacement of Al by Sb in Silmanal on the structure and magnetic properties was investigated also.

About 200 x-ray films and a number of diffractometer charts were taken from alloys of 15 different compositions in various states of heat treatment. Measurements of saturation magnetization, coercive force, Curie temperature and Rockwell hardness were made. In addition optical and electron micrographs, microprobe analysis and differential thermal analysis were carried out to supplement the x-ray analysis.

The magnetic properties in Silmanal are produced by a semi-coherent precipitate which was found to be of the L10 structure type with lattice parameters $a_0 = 3.94 \text{ \AA}$, $c_0 = 3.58 \text{ \AA}$. The phase precipitates from the supersaturated Ag-mixed crystal below 200°C and starts to decompose at 250°C , whereupon an Ag-rich, nonmagnetic, stable phase with a structure similar to β -Mn is formed.

The Ferromagnetic Phase in Silmanal

The magnetic phase has previously been identified as a polymorph of a MnAl compound, but was never found in Silmanal before. The kinetic characteristics of this phase in Silmanal are essentially different from those in the Mn-Al and Ag-Mn-Al system with low silver content, and are in causal relation with the supersaturation of an Ag solid solution.

Substitution of Ag in low-Ag alloys by Cu or Ni results in the formation of a ferromagnetic phase of the B2 structure type. The energy product, BH, of the Ag₅MnSb alloy is higher than that of Silmanal and still higher values might be obtained by increasing the relative amount of the ferromagnetic constituent.

The Ferromagnetic Phase in Silmanal
and Related Alloys

1. INTRODUCTION

Ever since the pioneering work of Potter (1) on the Ag-Mn-Al system in 1931, scientists have been intrigued by the extremely high coercive force $I_c H_c$ of the alloy Ag_5MnAl which with a value of 6000 Oe happens to be the highest of all known magnetic alloys.

The presence of a ferromagnetic intermetallic compound in Silmanal, an alloy consisting of one diamagnetic and two paramagnetic metallic elements refers the phase to an ever increasing interesting group of ferromagnetic manganese and chromium compounds. Both these elements form ferromagnetic phases with non-metals as well as with metalloids and non-ferromagnetic metals. This tendency can be explained on the ground of the Heisenberg concept of quantum mechanical exchange forces between the electrons of neighbouring atoms. The exchange forces, negligibly small for wider atomic separation, become effective at a distance of approximately 3.6 \AA , causing parallel alignment of the spin moments of neighbouring atoms. Gadolinium with interatomic distances of 3.573 \AA and 3.636 \AA (2) is the element with the widest atomic separation over which positive exchange forces manifest themselves in the parallel coupling of the unsaturated spins from the partially filled 4f shells. At these interatomic distances however, the energy of the exchange forces is still small and is overcome by the energy of thermal vibrations at a rather low temperature.

Thus, the Curie temperature of Gd is low, 290°K . The exchange energy increases with decreasing atomic separation and passes a maximum for a distance of approximately 2.51 \AA (3). The ferromagnetic element with atomic separations closest to this value is Co with $d_{\text{Co-Co}} = 2.50 \text{ \AA}$ (2) and with the highest Curie temperature among the elements, $\theta = 1400^{\circ}\text{K}$. When the energy of interaction is plotted against the ratio

$$\frac{R}{r} = \frac{1/2 \text{ interatomic distance}}{\text{radius of partially filled subshell}}$$

as in the curve of Bethe (4), (see Fig. 1) the Curie temperature θ of the ferromagnetic elements, on the absolute scale, appears connected with it by the relation $k\theta/Z = E_{\text{exchange}}$, where Z is the number of nearest neighbors and k is the Boltzmann constant. Similar curves can be drawn for series of intermetallic compounds, and it appears that the interaction energy is slightly dependent on the crystal structure. If the number of nearest neighbors is not the same in a series of compounds (as it is not the same for the series of elements in Fig. 1) θ is not exactly proportional to E_{exchange} . Nevertheless the curve shows clearly that the energy function crosses the zero line for a certain R/r value. Slater (3) calculated this ratio to be 1.50. The ratio for Mn with 1.47 lies below this value which separates the ferromagnetic from the non-ferromagnetic transition metals, and Mn is not ferromagnetic in the pure metallic state. The ratio is however close enough to the critical value that the increase of the Mn-Mn distances in compounds, where small non-metals like N i in Mn_4N (5),

P in Mn_2P (6), and B in MnB (7) become first-order neighbours of Mn atoms, is sufficient to bring it over the critical value and these compounds are ferromagnetic. Apparently, even solid solution of H in the Mn structure is sufficient to produce slight ferromagnetism (7). A great number of intermetallic Mn compounds with cubic, hexagonal or tetragonal structure types are ferromagnetic. The MnAl phase will be discussed in detail below. Ferromagnetic B8 phases were found in compounds with As, Bi, Sb and Sn. MnAs (8) and MnBi are of the simple $B8_1$ structure type where Mn occupies the equivalent positions 2a in 0,0,0 and 0,0,1/2. Additional positions 2d in 1/3, 2/3, 3/4 and 2/3, 1/3, 1/4 are half filled at the Mn rich boundary of the homogeneity range $Mn_{1+x}Sb$ with $0 \leq x \leq 0.5$ (9), and Mn_2Sn (10) is of the completely filled $B8_2$ type. In the latter system there is another ferromagnetic phase $Mn_{11}Sn_3$ (11) of the hexagonal DO_{19} type. A superlattice of the B8 phase was found in the Mn-Ge system as the ferromagnetic $D8_8$ phase by L. Castelliz (12).

An interesting group of ferromagnetic compounds are the Heusler phases. Cu_2MnAl has an ordered, face centered $L2_1$ type of structure (13) and Cu_2MnGa , Cu_2MnIn (14) and the high temperature polymorph of Cu_2MnSn (11) are isostructural with Cu_2MnAl . Castelliz (15) found a continuous transition from the cubic C1 phase $NiMnSb$ to the Heusler phase Ni_2MnSb in the course of which a fourth sublattice was filled with Ni. The increase of the Ni concentration is associated with a decrease of the saturation magnetization by more than 50% and a drop of the Curie temperature by more than $300^\circ C$. From the variation of

the magnetization and the change of the interatomic distances in connection with the change of the Curie temperature, the author concluded that Mn-Mn spin exchanges contributed most to the ferromagnetism in these compounds and that the Ni-Ni contribution was only small. Subsequently similar Cl and Heusler phases were found where evidence could be given that favourable Mn--Mn distances were mainly responsible for the ferromagnetism of the alloys, even in the presence of ferromagnetic elements. They were found in the systems Cu-Mn-Sb and Cu-Ni-Mn-Sb (16), Ni-Mn-Sn, Co-Mn--Sn and Co-Mn-Sb (12), Ni-Mn-In, Ni-Mn-Ga, Co-Mn-Ga and Pd-Mn-SSb (17).

Shortly after the discovery of the original Heusler phase by F. Heusler (18) and before the structure was analyzed by O. Heusler (13) and Bradley (19), H. H. Potter attempted to reproduce the structure by the replacement of Cu with Ag. The structural analysis of the Cu_2MnAl phase presented major difficulties because of the small difference between the atomic scattering factors of Mn and Cu. The valuable mechanical properties of the Heusler alloys which had received wide attention were expected to be retained by the replacement. On substitution Potter found that the maximum intensity of the magnetization arose not at Ag_2MnAl but at Ag_5MnAl . Fig. 2 shows Potter's results, redrawn to give contours of equal saturation intensity per cubic centimeter. The cross marks the position of Ag_5MnAl . The maximum intensity of magnetization was obtained by chill-casting and aging at 250°C for several days. The coercive force of this alloy for vanishing intrinsic induction, H_c was large,

about 5000 Oe, and not only greater than the values observed with other alloys, but of a different order of magnitude. Although H_c is small, and consequently the energy product is small, the alloy is of technical interest and is commercially known as Silmanal. This alloy combines ductile qualities with a resistance to demagnetization of more than ten times that of the strongest Alnico and can be subjected to strong alternating fields without loss of magnetization (20). Since Silmanal has a residual induction of only 600 gauss, the design of a magnet must provide a large cross-section to length ratio, a requirement which gave rise to a whole new breed of magnet-shapes such as diametrically magnetized wires and pancake magnets. Besides the technical interest, there was and still is considerable theoretical interest in the specific magnetic properties of the alloy and the structural conditions leading to them. Potter could not find the evidence of a second phase. The X-ray powder pattern taken from the alloy in this magnetic state showed only the pattern of a silver solid solution which could not be made responsible for the occurrence of ferromagnetism.

Twenty years after the first report about Ag_5MnAl , A. A. Geisler (21) studied the alloy. He came to the conclusion that Silmanal is a precipitation-hardening alloy rather than an alloy with an ordered structure of the Heusler type. Geisler detected two different precipitates in Silmanal, but attempts to identify these precipitates failed.

Petrow and Potemkin (22) investigated the Ag-Mn-Al system in 1957. They constructed the phase diagram of the Ag-rich section of the system by means of DTA, XRD, microstructure analysis, microhardness tests, magnetic measurement and specific electric resistance measurements. They established the existence of two phases in the neighbourhood of Ag_5MnAl , a solid solution of Mn and Al in Ag and a second phase which they thought to be a solid solution of Al in Mn. On the basis of their results the authors concluded that the Ag mixed crystals decomposed whereby a ferromagnetic phase separated as an incoherent precipitate with particle size below the scope of optical resolution and x-ray diffraction. Petrow and Potemkin, supported by the fact that permanent magnetic alloys with high coercive force often form solid solution precipitates (23) (24), assumed that the unidentified decomposition product in its initial stage is a solid solution of Al in Mn.

The most detailed work was carried out in 1958 by E. O. Hall (25) who introduced electron diffraction work to the study of $Silmanal$. He established the approximate ternary diagram of the Ag-Mn-Al system at $650^{\circ}C$ and $400^{\circ}C$. His investigation showed that the magnetic alloys of the system lie in the binary field of α -Ag and β -Mn and the author suggested that the ferromagnetic phase is a non-equilibrium nucleation phase which forms on aging from the supersaturated silver matrix, grows into a Widmanstätten structure and eventually transforms

above the Curie point into the equilibrium product β -Mn. Attempts to extract the ferromagnetic precipitate by electrochemical means failed, but a carbon replica extraction technique was successfully developed. Electron diffraction patterns were obtained from the carbon replica of magnetic and non-magnetic samples. The precipitate of the latter, aged at 400°C , was recognized as predominantly consisting of β -Mn with $a_0 = 6.39 \text{ \AA}$. The precipitate of a magnetic specimen aged at 240°C produced an electron diffraction pattern, the d-values of which are given in the paper. Calibration of the pattern with evaporated thallium chloride and trial plotting with Bunn charts showed a possibility of indexing the diffraction rings as the diffraction pattern of a primitive hexagonal cell. Hall calculated the parameters with $a_0 = 2.94 \text{ \AA}$, $c/a = 1.61$ and claimed the phase, designated ξ' , to be the ferromagnetic constituent.

Apart from the ambiguity with which the solution of a diffraction pattern with Bunn's charts is affected, Hall's results on the ferromagnetic phase do not appear very satisfactory. It is not intended to apply adverse critique to the work of Hall which indeed has to be regarded as the most substantial contribution to the knowledge of the kinetics of phase transformation in this complex system. Only the specific question about the chemical nature of the ferromagnetic phase and its relation to the other phases of the alloy is not answered by the given results, even if the reality of the ξ' phase is assumed. This latter point will be discussed with the results of the present work.

From the brief survey of previous studies of Silmananal it is apparent that there is much uncertainty about the structure and the chemical nature of the ferromagnetic phase in this alloy. The results quoted by different authors are at variance and agreement exists only with regard to the difficulty of this investigation. It seemed however that in all the efforts made so far x-ray diffraction was not used to its full capacity of detecting small crystal aggregates. An effort in this direction seemed justified not only for theoretical but also for economical reasons. Any attempt to approach the valuable magnetic properties of Silmananal in a less expensive alloy can only start with the detailed knowledge of the nature of its ferromagnetic constituent.

2. EXPERIMENTAL

2.1 Materials

High purity silver rod (5N), manganese flake (4N5), antimony shots (5N) supplied by Koch-Light Laboratory Ltd., Bucks, England, aluminum (4N8) supplied by Aluminum Company of Canada Ltd. and nickel (4N8) and copper (5N) rod from Johnson Matthey and Company Ltd. were used for the preparation of the evaluated Sillmanal and related alloys. Trial runs for melting and casting and for the preliminary testing were carried out with metals of lower purity.

2.2 Preparation of Samples

The charge was melted in a recrystallized alumina crucible by induction heating in argon gas and then cast in a copper mold inside a Balzers vacuum melting and casting furnace powered by a Philips high frequency type PH 1012/21 generator.

Measured amounts of silver, manganese and aluminum (86.9% Ag, 8.8% Mn and 4.3% Al) having a total weight of about 25.5 g were placed in layers in a crucible. Mn, being the component with the highest melting point, was placed between Ag layers. The bottom layer was formed by silver, and the topmost layer by aluminum. The principle of this arrangement was that the aluminum, being first to melt, would flow downwards and react with Mn and Ag thereby reducing their melting temperature.

One layer of graphite felt was placed around the crucible which in turn was covered by alumina felt for thermal insulation.

The crucible with the felt was then placed in the water cooled copper induction coil. The system was evacuated to 1×10^{-5} mm pressure before flushing it with high purity argon gas. The system was then heated to about 400°C and evacuated again to expel air or gases trapped in the felt. The chamber was filled with argon gas at 0.9 atmospheres pressure after a vacuum of 5×10^{-6} mm was attained. The alloy was then melted by induction heating and cast in a split copper mold (1 in. x 1.7 in. x 4 in.) with a 1/4 in. diameter bore of 2.5 in. length. The casting operation was performed in the chamber by tilting the induction coil along with the crucible by means of a handle operated from outside.

A similar procedure was adopted for the preparation of Mn-Al binary and Mn-Al-Ag, Mn-Al-Cu, Mn-Al-Ni and Ag-Mn-Sb ternary alloys with the exception that commercially pure argon gas was used instead of high purity argon gas. The alloys including Silmanal were kept in the molten condition for as short a time as possible in order to reduce to a minimum the evaporation of Mn and to prevent the formation of blow-holes.

Homogenizing

The cast samples were sealed in silica tubes with high argon gas to minimize evaporation. Direct contact of the samples with the tube was avoided by placing broken pieces of alumina between the sample and the wall of the tube to avoid contamination. The sample

was given a pre-homogenizing treatment at low temperature. It was then homogenized for at least twelve hours at a temperature close to the solidus line at the given composition and quenched.

Aging

Alloys were aged at various temperatures. The samples, either in the form of the rod as cast, or rolled to sheets of 0.05 mm thickness, or filed and ground to powder of -325 to +200 mesh-size were sealed in vycor tubes with argon gas. Alumina felt was used between sheets when more than one sample was sealed in the same tube. A box-type muffle furnace with a maximum temperature fluctuation of $\pm 2^{\circ}\text{C}$ was used for the aging treatment.

Some of the Silmanal alloys were aged in the magnetic field of a horse-shoe type permanent magnet with a field strength of 1700 Oe. A narrow furnace of one inch outside diameter was built to fit inside the space between the poles. It consisted of an insulated heating coil in the form of a spiral tube and was placed inside a water cooled copper tube of one inch diameter. The outside shell of the furnace had to be cooled during the procedure in order to protect the magnet. The temperature fluctuations produced by the cooling device were minimized by modifying the temperature control of the furnace in such a way that a delay relay produced an overcharge during the first three seconds of energization. With the aid of this arrangement the temperature was controlled to $\pm 2^{\circ}\text{C}$ in the range between 200°C and 250°C .

2.3 Chemical Analysis

The composition of the alloys was determined in the following way. About one gram sample was dissolved in 50% nitric acid. Ammonium chloride was then added to separate silver by precipitation. The precipitate was washed, dried and weighed. Aluminum was then separated by precipitation from the filtrate by ammonium hydroxide. The precipitate was dried and then burnt for the determination of the amount of aluminum. Extreme care was observed to avoid the precipitation of manganese along with aluminum, by controlling the acidity of the solution to pH 6.5. Manganese was then separated from the filtrate by precipitation with the help of ammonium phosphate. The accuracy of this method was tested on standard solutions. The deviations were found to be not greater than ± 0.2 , ± 0.7 and ± 0.7 wt % for silver, manganese and aluminum respectively.

2.4 X-ray Investigation

Powder diffraction photographs were taken in Straumanis-type powder-diffraction cameras with nominal diameters of 114.6 mm, using Kodak no-screen medical x-ray type film. The x-ray generators were Philips PW 1009 and PW 1010/30 with hot-cathode tubes. Filtered characteristic K radiations from cobalt and copper target were used, depending on the composition of the individual samples.

A Norelco vertical-scan diffractometer was used for quantitative analysis. A proportional counter and a pulse-height analyzer permitted an optimum adjustment of the peak-to-background ratio. Slits of

different angular widths made accessible a range of 2θ values from 10° to 162° without distorting the diffracted intensity. The circuitry associated with the diffractometer made it possible to record the diffraction patterns on a strip chart or to accumulate counts for predetermined times.

Powder Photography

Extreme care was observed during the preparation of the powder samples to avoid contamination. The test samples were prepared by filing and grinding to pass 325 mesh. The diffraction lines were measured with a device equipped with a vernier reading to $1/50$ mm. The Bragg angles were corrected for the actual length of the film. The final lattice parameters were found by the use of the Nelson-Riley function.

X-ray Diffractometry

Diffractometry (using powder or sheet samples) was used for the identification of phases and for the quantitative determination of intensities. The counter technique permitted integrated intensities to be measured more accurately than is possible with the photographic method since it does not depend on the film characteristics and the processing, and the specimen area from which the diffracted intensity is obtained is larger, thus resulting in a better averaging.

The powder samples were prepared either by pressing the powder (-325 mesh) into the shallow counterbore of a one inch diameter aluminum slug or by placing a paste made by mixing the powder with

a little silicone grease into the shallow counterbore of a lucite slug. The sheet samples were firmly placed on the lucite slug with a small amount of silicone grease.

The base and the channel width of the pulse-height analyzer were adjusted to an optimum peak-to-background ratio with the aid of an energy distribution scan for the strongest peak of the diffraction pattern.

The individual integrated intensities were obtained by counting while scanning at $1/8^\circ (2\theta)/\text{min.}$ across the peak, allowing for generous portions of background on both sides of the peak. A suitable background count would then be subtracted from the total count, assuming linearity of the variation of the background intensity under the peak. The counting was repeated three times for each peak, aiming at reduction of the spread below 5%.

2.5 Magnetic Measurements

Hysteresis Loop

A "Four-Inch" Varian electromagnet model V-4004 with a model V-2300A power supply and a model V-2301 current regulator supplied the magnetic field in which the measurements were carried out. The field was calibrated as a function of current, pole distance and the distance from the central line connecting the pole caps by means of a Bell 640 Incremental Gaussmeter and a Probe Model T6001. The changes of the magnetic induction by changes of the magnetic field were registered by a Leeds and Northrup ballistic galvanometer type H.S. The

characteristic sensitivity of 0.003 microcoulomb per mm n at one meter distance and a period of 25 seconds were specified for this galvanometer. The deflections were measured on a curved scale of 1 m radius.

The specific magnetic properties of Silmanal, a verery high coercive force $H_c = 6000$ Oe combined with a low saturation magnetization $4\pi I_s = 880$ gauss produced experimental diifficulties. The saturation field strength lay between 16000 and 2000000 Oe and consequently, a field change of several thousands of oersted produced only a small change of the magnetization and h hence only a small deviation of the galvanometer mirror. In order t to increase the sensitivity of the measuring device the pole distance had to be kept as small as possible and the number of windings onn the pick-up coil had to be made as great as possible. The effect o of the field changes on the pick-up coil was compensated by a secondnd coil of equal geometric dimensions wound in the opposite sense e and mounted as close as possible to the sample coil.

The experimental procedure was as follows. The sasamples were machined to rods of 10 mm length and 3 mm diameter and id placed in the pick-up coil. The latter consisted of a plastic s spool with 3 mm inside diameter wound with 320 turns of 36 gauge enamelled copper wire. The compensating coil was prepared in the same ve way. The two coils were mounted side by side on a perspex stand riggigidly fixed to the base plate of the magnet. This arrangement secured the position

of the sample in the center of the 11 mm pole distance. The arrangement is shown in Fig. 3. Ideal compensation was very difficult to obtain. Minute differences in the mode of winding and in the position of the exit wires of the two coils with respect to the field lines easily offset the balance. Therefore, a third coil with a few turns was connected in series with the sample coil and mounted above the central line of the twin coils with its plane parallel to the field lines (see Fig. 3a). The final adjustment was provided by a slight rotation of the auxiliary coil.

The galvanometer had to be carefully shielded from the direct influence of the field. It was placed at a distance of approximately eight feet from the magnet and the extension wires were braided to compensate stray fields.

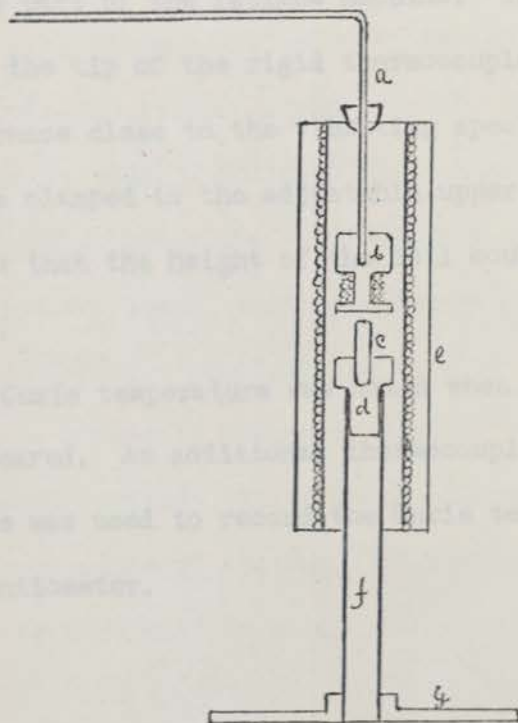
The measurements were carried out in the following way. The sample was saturated in a field of 20,000 Oe, obtained with 3 inch polecaps at a distance of 11 mm. The galvanometer circuit was open during the process of saturation. The field was then set at a given value with the aid of the current regulation, and the $\Delta I = I_{sat.} - I_1$ produced in the sample by a $\Delta H = H_{sat.} - H_1$ was measured. In this manner the individual point of the hysteresis loop from $+H_{sat.}$ through $H = 0$ to $-H_{sat.}$ were found and the curves constructed.

The apparatus was calibrated for absolute I values with a specimen of pure nickel of identical dimensions, the saturation magnetization of which was taken as 500 gauss.

Curie Temperature

A makeshift arrangement composed of equipment available in the Departments of Mineral Engineering and Chemical Engineering was used for the Curie point measurements.

Samples of about 6 mm diameter and 20 mm length were used for the Curie point measurements. The top end of the sample was slightly tapered to prevent it from hitting the coil when ascending. The specimen was saturated in the Varian magnet at 2000000 Oe and fitted into the upper end of a silica tube by means of a teflon sleeve as shown in the sketch below.



- (a) Thermocouple Sheath
- (b) Pick-up Coil
- (c) Sample
- (d) Teflon Sleeve
- (e) Furnace
- (f) Silica Tube
- (g) Base

The silica tube was fixed rigidly to the vibrating platform of a fatigue machine (Fig. 4a). A pick-up coil with 200 turns of teflon coated 32 gauge copper wire was wound on a teflon spool and connected with an Analab Dual-Trace Oscilloscope, Type 1120. The position of the coil with regard to the sample was adjusted in such a way that the end of the sample stayed about the central position of the coil, whereby the coil received the maximum effect of the change of flux lines produced by the vibrating specimen. The frequency of oscillation of the fatigue machine and the amplification of the oscilloscope were adjusted to give a clear and well observable sine signal on the screen. Heating of the specimen was accomplished by means of a noninductively wound tube furnace fixed to the stationary part of the fatigue machine. The pick-up coil was fitted on the tip of the rigid thermocouple sheath and inserted in the furnace close to the vibrating specimen. The thermocouple sheath was clamped to the adjustable upper platform of the fatigue machine so that the height of the coil could be conveniently chosen as needed.

The Curie temperature was noted when the curve decreased suddenly or disappeared. An additional thermocouple which was touching the sample was used to record the Curie temperature more accurately by a potentiometer.

2.6 Hardness Measurements

Silmanal samples of 6 mm diameter and 6 mm length were used for the hardness measurements performed by a Rockwell hardness tester. One-sixteenth inch diameter indenter at 100 kg load was used to get the hardness on the B-scale.

Considering the fact that the precipitated phases in Silmanal are extremely small and the sample is polycrystalline, the results of macrohardness tests were considered as a more realistic representation of the physical characteristics of the alloys than that of microhardness tests.

2.7 Metallographic Examination

Silmanal samples for microscopic examination were prepared by polishing with diamond pastes of different grades (6, 1, 1, and 0.25 micron). The final surface was prepared by polishing with 0.05 micron alumina powder, followed by etching in five percent potassium cyanide-ammonium persulphate solution or acid ferric chloride.

The preparation of these samples was very tedious, because of the presence of hard precipitates in a soft silver matrix. Despite extreme care a certain amount of pitting could not be avoided.

Polished sections of the other alloys, binary Mn-Al or with small concentration of Ag, Cu or Ni, were easily prepared as the hardness was more uniform over the entire specimen.

2.8 Electron Microscopy

A Philips EM 300 electron microscope was used to study the structure of Silmanal precipitate by the following methods:

- (a) Transmission electron microscopy
- (b) Extraction replica method
- (c) Magnetic colloid method

Thinning of Samples for Electron Transmission Technique

Attempts to prepare specimens for electron transmission studies were most disappointing. Several methods of thinning were tried without much success. They are compiled in a list on page 21. Specimens used for thinning were sheets of 1 to 3 thou thickness.

Carbon Replica

The surface of Silmanal samples was prepared by light etching in 5% potassium cyanide-ammonium persulphate solution. The surface contamination was eliminated by the use of an acetylullose film. The film was deposited on the surface wetted with methyl acetate and then stripped after drying (29). A carbon film was then deposited on the clean surface. After a second etch the carbon replica film was separated by stripping, using a backing layer of Duco cement as a support. The sample was cut to the required size and the Duco cement was removed by ethyl acetate.

Process	Solution	Condition
1. chemical thinning	20% nitric acid	room temperature
2. electro-chemical thinning		
a) disa electropolishing	butylcellosolve 50 ml ethanol 350 ml perchloric acid 40 ml water 60 ml	20-30 volts room temperature
b) Bollman electrothinning (26)	ethyl alcohol 80% perchloric acid 20%	room temperature 10-20 volts
c) electro-chemical jet after Hugo and Phillips (27)	20% nitric acid	room temperature
d) modified window after Glen and Raley (28)	KCN 17 g K-ferrocyanide 3.75 g K-tartarate 3.73 g phosphoric acid 3.5 ml l ammonia 1.0 ml l water 250 ml l	6-8 volts room temperature stainless s.cathode
e)	chromic oxide 150 g glacial acetic acid 750 ml l water 30 ml l solution was heated at 65°C one hour under constant stirring	room temperature 10-12 volts
f)	80% absolute alcohol 20% perchloric acid	-30°C 10-20 volts

Only method f produced a specimen which was, at least in a small area, thin enough for electron transmission. With the other methods the sheets became perforated long before the necessary thickness reduction was obtained.

The Dried Colloid Technique

The dried film method suitable for recording static domain pattern was used in an attempt to reveal ferromagnetic domain pattern in some of the alloys.

The magnetic precipitate, colloid magnetite, was prepared by a method described by Elmore (30). The precipitate was added to 0.1N HCl. When it was peptized to form a dense colloid, a solution of celacol was added to bring the final concentration of magnetic colloid to a value of between 0.5 and 1%. Finally glycerine in an amount of approximately 10 wt % of celacol was mixed into the liquid. Then the colloid was dialyzed against distilled water through a cellophane membrane to remove the excess chlorine, filtered and diluted until a deep amber color was obtained.

2.9 Differential Thermal Analysis (DTA)

Powder samples from quenched alloys were examined by a Deltatherm Model d2000-16 analyzer in a temperature range from room temperature up to 500°C. The heating rate was 12°C per minute. The instrument had four channels which allowed the recording of two duplicate samples at the same time.

3. RESULTS AND DISCUSSION

3.1 Phase Relation in the Binary Mn-Al System in the Vicinity of MnAl

In the early stage of the work some of the x-ray films taken from Silmanal aged at 240°C showed, besides the lines of the Ag-matrix, one faint line which could be interpreted as the strongest line of a phase which was quoted by Kono as one of the MnAl polymorphs.

Horoshi Kono (31) reported in the Journal of the Physical Society of Japan in 1958 that a metastable ferromagnetic phase is formed when the loose-packed hexagonal h-phase of a Mn-Al alloy with approximately 55 at % Mn is cooled from 950°C to room temperature, and a cooling rate of 10°C/s is maintained in the region of approximately 800°C. The Curie temperature of this phase is about 380°C. This metastable phase has a tetragonal structure with parameters of $a_0 = 3.94 \text{ \AA}$ and $c_0 = 3.58 \text{ \AA}$. Only an alloy with 55.1 at % Mn was homogeneous after cooling, containing just the ferromagnetic phase.

In alloys with higher Mn content β -Mn was present besides the ferromagnetic phase. In alloys with higher Al content lines of another phase, the product of a eutectic reaction occurring at 840°C, were observed besides the pattern of the ferromagnetic phase. Structural analysis of the latter phase was quoted by Kono to be difficult and no diffraction lines were given. In 1960 Koch et al (32) claimed the discovery of a new metastable phase of a tetragonal structure in the Mn-Al system and called it ζ -phase. It has the approximate composition $\text{Mn}_{1.11}\text{Al}_{0.89}$ and can only be obtained by cooling the

sample from 825°C to 600°C at a critical rate of approximately 30°C/s. The lattice parameters of this phase were given as $a_0 = 2.77 \text{ \AA}$ and $c_0 = 3.57 \text{ \AA}$.

There is little doubt that the phase reported by Koch et al. is identical with Kono's phase, but referred to a smaller unit cell.

Between the parameters of the two cells the relations exist:

$a_{\text{Koch}} = 1/\sqrt{2} a_{\text{Kono}}$ and $c_{\text{Koch}} = c_{\text{Kono}}$, thus the a-axis of Koch's b.c. tetragonal cell is equal to half of the base diagonal of Kono's f.c. tetragonal cell. Koch et al. assumed that Al and the excess of Mn over Al occupy the 1/2, 1/2, 1/2 lattice positions but did not do quantitative structure analysis. The standardized relative intensities of the phase reported in ASTM card 11-520 do not agree with the intensities given in the original paper of Kono.

The occurrence of the tetragonal phase in Mn-Al alloys at about the composition Mn Al was studied using the heat treatment which, according to previous investigations (1, 21) provided the optimum magnetic properties in Silmanal. Results of this study are given in Tables 1 to 5. In Table 1 the effect of the quenching and aging temperatures on the phase relations of alloys with slightly different compositions, and the correlation between the structural state on the one hand and the magnetic and mechanical properties of the alloys on the other hand, are shown. The τ -phase was obtained in all air-quenched samples regardless of the slight difference in the Mn concentration. None of

the alloys was homogeneous, containing τ -phase only, but the h-phase was always present, although in a very small quantity. . This indicates that in the Silmanal treatment the temperature range in which the h-phase of the binary alloy decomposes is passed so fast that the decomposition is not completed. The relative intensities of the β -Mn phase depended on composition and quenching temperatures, but showed no distinct correlation with the aging temperatures. The only x-ray specimen giving τ -phase only was the magnetic fraction of sample 3 which was separated from the powdered (250 mesh) sample by an alnico magnet. Table 1 shows that the ferromagnetic constituent is unambiguously the τ -phase. The table also demonstrates that alloys containing τ -phase are resistant to impact in spite of the presence of the brittle β -Mn phase.

Estimated intensities and interplanar spacings of the x-ray reflections, given by the three phases of sample 7 listed in Table 1, are shown in Table 2, together with the relative intensities according to the ASTM cards. That a relation exists between the structure of τ and h phases becomes evident by the coincidence of two strong reflections

$d_{\tau}(111) = d_h(002)$. Another coincidence of reflections occurs with

$d_{\tau}(201) = d_{\beta\text{-Mn}}(321)$.

In Tables 3, 4 and 5 the experimental d-values of τ -phase, h-phase and β -Mn-phase are compared with the values of the respective ASTM cards. Whereas the experimental spacings in the first two phases are very close to Kono's values compiled in the cards, the spacings

in β -Mn refer to a cell axis which is greater by approximately 2% than the values given for pure β -Mn. The following values are all converted to angstroms.

a_0 of β -Mn in \AA	Reference
6.3018	ASTM No. 1-1234, Zwicker et al. (1949)
6.3036	Pearson (loc. cit.), page 735 Johannsen and Nitka (191938)
6.3144	Pearson (loc. cit.) Table 7
6.313	Barrett (33)
6.426	Present work for $\text{Mn}_{1.2525}\text{Al}$
6.388	Present work for MnAl

Solid solution of Al in β -Mn increases the lattice constant of β -Mn. Data from Zwicker (1951) are given in Pearson (1 (loc. cit.) according to which a solid solution of 18.4 at % Al increased the lattice parameter to 6.383 \AA , which is still lower than the values obtained in the present work. The value obtained by Bradley and Jones (34) was however very close to the value in the present work. The lattice constant of the solid solution of Al in β -Mn was determined by them to be 6.41 \AA . From this value, used in conjunction with Vegard's law, they determined the approximate percentage of Al to be 25 at %. Lower a_0 values for β -Mn were found in stoichiometrically prepared AlMn.

3.2 Phase Relation in Silmanal

Powder Specimens

The analysis of the structure of the ferromagnetic phase in Silmanal was the most important part of this work and a great deal

of time was spent developing the most suitable procedure, i.e. The task was to find evidence of the structure of a probably fine-grained precipitate which was stable in a narrow temperature range only and which was always accompanied by the silver matrix and at least one other phase.

The preparation and heat-treatment of the x-ray specimens and the final choice of the x-ray procedure were carefully tried out. Although it would have been preferred to apply the aging treatment to the homogenized and quenched bulk sample, in a great many cases it was necessary to perform the aging on sample filings. This necessity occurred when samples were investigated that were aged below 300°C . In order to relieve the stress introduced during filing the samples had to be treated at 300°C for five hours. Annealing at this temperature following an aging treatment at 240°C annihilated, of course, the specific effect of the lower temperature. Annealing at 220°C over a period of one week did not stress relieve the filings sufficiently to produce sharp diffraction lines. The general procedure which was followed when the precipitation below 300°C was studied was to prepare filings from the quenched rod and perform simultaneously aging and stress relief of the x-ray specimens in an argon filled pyrex tube at controlled temperature, i.e.

Mo, Cu, Co and Fe radiations were investigated with regard to the detectability of the weak lines of the precipitated phase. It was found that of the latter three sources CuK α radiation produced the best contrast in spite of the slightly higher background

originating in the fluorescent radiation from Mn, and more lines could be detected. Mo radiation did not provide sufficient resolution of closely spaced lines belonging to different phases. Small camera films were used for an initial information but the films designed to be measured were taken in 11.4 cm cameras. After many trials an exposure time of 12 to 15 hours, with the high voltage reduced to 34 KV and overdeveloping of the film in a weak developer, produced the maximum number of lines of the precipitates. In this way at least five reflections could be detected and identified as belonging to the ϵ -phase of the Mn-Al system which has been discussed in the preceding section. At the beginning of the work when the films were exposed 5 hours, only (111), the strongest reflection of the pattern was faintly discernible from the background. Since however with this exposure time the lines of the Ag matrix appeared nearly solarized, it is understandable that previous investigators of Silmanal did not attempt to experiment with still longer exposure times. It was, in fact, the perfect agreement of the faint (111) line with the strongest line of Kono's MnAl phase which determined the direction of the present investigation.

In Table 6 the complete x-ray pattern of an Ag_5MnAl alloy aged at $240^\circ C$ is given. The actual composition of the sample as found by chemical analysis, with 86.82 for Ag, 8.78 for Mn and 4.40 for Al, given in wt %, compared very well with the nominal composition 86.9, 8.8 and 4.3 wt % respectively. This good agreement was

representative for all analyzed Silmanal specimens when the casting and homogenizing was carried out in argon under approximately atmospheric pressure. Two phases could be identified besides the Ag matrix. The β -Mn phase is represented with at least five reflections with relative intensities down to $I/I_0 = 20$. Although there is a coincidence of the (310) reflection with the (200) of Ag the presence of the weaker reflections of this phase leave no doubt about its contribution to the diffraction line with $d = 2.0370 \text{ \AA}$. The tetragonal phase of the Mn-Al system is also represented with at least five reflections, one of them coinciding with the (222) of Ag. Another reflection (201) is overlapping with the (321) of β -Mn and there is no way of estimating the relative contribution of each of the two phases to the reflection with $d = 1.718 \text{ \AA}$. According to the relative intensities calculated by Kono the (201) reflection of the γ -phase would hardly become recognizable. However K Kono, when calculating the intensities on the basis of a "CuAu type superstructure", which apparently is to be understood as the $L1_0 = \text{CuAu}$ I structure type, had to make an additional assumption about the lattice positions of the excess Mn atoms in the compound. He assumed that the excess Mn is substituting for Al. The equivalent lattice positions taken up by the elements of the compound $\text{Mn}_{1.23}\text{Al} = \text{Mn}_{1.115}(\text{Mn}_{0.115}\text{Al})$, or, referred to the 4 atoms in the cell, $\text{Mn}_2(\text{Mn}_{0.103}\text{Al}_{0.897})_2$ could then be given as

0.897 Al_I in 1 a 0, 0, 0

0.897 Al_{II} in 1 c 1/2, 1/2, 0 fo for assumption I

2 Mn in 2 a 0, 1/2, 1/2; 1/2, 0, 1/2

0.103 Mn either distributed statistically over br 1 a and 1 c or preferentially occupying positions in every second laylayer of Al atoms.

Another possibility would be a solid solution with ah a defect structure with vacant Al sites. Equivalent positions taftaken up by the elements of the compound Mn_{1.23}Al = MnAl_{0.81} would bd be as follows:

0.81 Al_I in 1 a

0.81 Al_{II} in 1 c for assumption II

2 Mn in 2 c

A calculation of the structure amplitude of the (20(201) reflection under assumption I and assumption II leads to an intensinsity ratio of $I_{II}/I_I = 2.4$. The possibilities for accommodating the ee excess Mn are of course not exhausted with these two assumptions, althlthough they might be the most probable ones, and an interstitial sol solid solution is excluded because of the atomic radius of Mn Mn being only some 20% smaller than the Al radius. However what mattatters for the present discussion is the fact that the calculated relatlatve intensities turn out differently for different assumptions, since ite it will be only the reflections with mixed indices the intensities of wif which are affected by the relative distribution of Mn and Al atomstoms over the lattice sites.

From the above discussion it might become sufficiently evident that the experimental intensity of the (201) reflection might be higher than the value calculated by Kono and that the ζ -p'-phase will therefore contribute to the experimental line with $d = 1.1.718 \text{ \AA}$. This would increase the number of ζ -phase reflections identified in the Silmanal alloy aged at 240°C to six. It should be stressed however that the evidence for the ζ -phase in Silmanal does not depend on the acceptance or rejection of a weak line as a line belonging to the structure. The evidence is rather given by the presence of all the lines with indices all even or all odd, with the exception of (002) and (220) for which Kono calculated the relative intensities with 14,5 and 17 respectively. In powder patterns of Silmanal alloys aged at lower temperatures or treated in a special way even more lines of the ζ -phase could be identified and this will be discussed further below.

The lattice constant of the Ag mixed crystal in the alloy of Table 6 was determined by Nelson-Riley extrapolation to be $a_0 = 4.0796 \text{ \AA}$ which was lower than that of pure Ag. Still lower values were found in Silmanal aged at higher temperatures. The implication of the heat treatment on the solid solution of Mn or Al in Ag, as revealed by the lattice parameter of the latter, will be discussed with Table 8 below.

In addition to the three phases identified in Table 6 a small amount of the hexagonal h-phase might be present in the Silmanal

alloy. Since two of the strongest reflections of this phase with $I/I_0 = 100$, $d = 2.05 \text{ \AA}$ and $I/I_0 = 80$, $d = 2.33 \text{ \AA}$ are very close to the heavily solarized Ag lines and a third one with $I/I_0 = 80$ and $d = 2.19 \text{ \AA}$ is coinciding with the (111) of the ζ -phase their presence may not be entirely excluded. However no trace is found of several clearly separated reflections with $I/I_0 = 50$.

In Table 7 the relative abundance of ζ and β -Mn phases is given, as estimated from the intensities and number of lines representing the two phases in the powder patterns of Si11 alloys aged at various temperatures. The precipitation of the tetragonal phase was predominant for aging temperatures below 240°C producing the (110) reflection with $d = 2.77 \text{ \AA}$ additional to the lines given in Table 6. It was approximately equal to that of β -Mn at 240°C and 250°C , and the precipitate disappeared at temperatures of and above 260°C . In powder patterns taken from samples in the quenched state no trace of the ζ -phase could be detected but β -Mn was represented by one very weak line. All samples in which ζ -phase could be traced were found to be ferromagnetic by a qualitative test. Aging performed in a magnetic field of 1700 Oe for 168 hours had no influence on the precipitation of the tetragonal phase. The effect of a double heat treatment on the phase relations was also investigated and the results are shown for the last two specimens in Table 7. As expected, neither was the ζ -phase when precipitated at lower temperatures preserved after subsequent aging at 400°C , nor could the effect of the

higher aging temperature be reversed by subsequent treatment of 240°C.

The results of the aging experiments, given in Table 7 might be interpreted in the following manner. The τ -phase precipitates in a temperature interval between 200°C (or slightly lower) and 250°C and redissolves at higher temperatures. Changes in the lattice parameters and the relative intensities of the phases which remain stable after the disappearance of the τ -phase could give information about the manner in which the phase is consumed. The accuracy with which the lines of the β -Mn phase could be measured was as high enough to calculate the d-values of individual reflections up to the third decimal. Within this accuracy no change in a_0 up to 240°C, but an increase of a_0 between 240 and 300°C could be detected and together with an increase of the intensities of the β -Mn reflections as relative to the Ag reflections. They increased by a factor of three as can be seen from the list below where the intensities measured on diffractometer charts are compared.

Silmanal sheet samples aged for 7 days.

Aging Temp. T°C	Relative Intensity	
	Ag (200)	β -Mn (310)10)
240	40	1
300	38	3

The lattice constant of the Ag mixed crystal, on the other hand, definitely decreased in the critical temperature interval in which

the γ -phase disappeared. This is shown in Table 8. The lattice constant for the pure silver metal $a_0 = 4.086_3 \text{ \AA}$, which is in very good agreement with the ASTM datum and the value of Pearson (loc. cit.), seemed to be lowered in the quenched state, but could not be measured accurately. It assumed a value of 4.079_6 \AA after aging at 240°C and decreased at the higher aging temperature by approximately 0.1%. The Ag lattice tolerates substantial amounts of Al or Mn in solid solution whereby, according to Pearson, the lattice constant decreases linearly with increasing Al concentration at a rate of 0.0013 \AA per 0.01 mole fraction replacement. The effect of Mn on the Ag parameter is much more complex. The a_{Ag} increases with the Mn concentration up to a maximum of 4.086_3 \AA for 5 at % Mn from which point it decreases slowly, passing the value of pure Ag, 4.086_0 \AA , at 15 at % Mn. A sharp descent between 15 and 19 at % Mn brings the a_0 value of the latter concentration down to 4.083_8 \AA and is followed by a much slower and linear descent which terminates with 4.079_0 \AA at the Mn-rich phase boundary at 39 at % Mn.

From the above description it becomes apparent that the observed decrease could not be produced by Mn alone, but rather by Al or by a joint effect of both Mn and Al. It may also be considered that, as a consequence of the precipitation and the subsequent breaking away of the precipitate the distribution of the solute within a silver crystal will be far from uniform

and it is not known when equilibrium will be reached after the τ -phase disintegrated between 240°C and 400°C . In Section on 4 the phase relations will be further discussed.

Besides Debye-Scherrer films, diffractometer charts were taken from Silmanal filings pressed or mixed with vacuum grease and spread on aluminum slugs. Tests were made with filings of different mesh size and they confirmed that the sieving did not imply a separation of grains of different composition. The relative intensities of the three phases present were not dependent on the size of the filings due to the very small crystallite size of the precipitates. The uniform distribution of the precipitates over the Ag matrix, and probable parent phase, is also evident from the fact that at a magnetic separation could not be obtained, whereas, in binary alloys the magnetic τ -phase could be separated from β -Mn, as it was discussed with Table 1. When the diffractometer specimens of an alloy aged at 240°C were exposed to a high magnetic field all the individual filings were seen to rotate in the direction of the field. Thus each of the filing particles consisting mainly of silver, and having the appearance of silver, contained the ferromagnetic component. The orienting effect of the field was caused by the shape anisotropy of the elongated filings. The contribution of a possible de crystal anisotropy in the tetragonal ferromagnetic crystals to the orienting effect could neither be proved nor ruled out. Comparing the peak areas of the Ag reflections on diffractometer charts it was found

that the relative intensities of the Ag-phase were different in magnetic specimens when compared with specimens of pure Ag, prepared exactly the same way. This observation was not studied in more detail, but it might be caused by the combined effect of oriented precipitation of the ζ -crystals on the Ag-crystals with crystal anisotropy in the ζ -crystals. The crystallographic relationship expressed by the coincidence of $(311)_{\zeta} = (222)_{Ag}$ very likely indicates the precipitation of the ζ -crystals with the (311) plane parallel to the (111) plane of Ag. Although nothing is known about the anisotropy of the ζ -phase and although the oriented precipitation of the ζ -phase is not as certain as it is with the β -Mn phase (see Section 4) the above explanation of the change in I/I_0 appears more probable than the assumption of a preferential substitution of Ag atoms by solute atoms in selected lattice points of the f.c.c. Ag lattice. A further investigation of these observations, especially of the I/I_0 in Ag as a function of aging temperature, could be expected to help clarify the complicated phase relations in these alloys.

With respect to the evidence of precipitated phases fewer reflections were recognizable amidst the background noise on the charts than were visible on the films. Various settings of scale factor and pulse height analyzer were tried out for an optimum peak/background ratio. This ratio was noticeably better with sheet specimens.

Sheet Specimens

After quenching, some of the Silmanal rods were cold rolled with a reduction of 80% to sheets of 0.003 in thickness. The sheets were either used directly as diffractometer specimens or cut into strips which were used as camera specimens. In the latter case the strips were treated with dilute nitric acid to remove the strained edges and reduce the strip further to a wire of approximately circular cross section of 0.05 mm. After the treatment the surface was thoroughly cleaned with fine emery paper. The same aging treatment was applied to sheet and strip specimens as described for the powder specimens.

The powder patterns obtained from wire specimens gave the same number of lines of precipitated phases as the films taken from filings which were given the same heat treatment and thus the wire specimens were not superior to powder specimens in this respect. They became however a valuable tool for the study of the effect of chemical treatment on the Silmanal structure that will be discussed below.

Sheets as diffractometer specimens were used for easy comparison of special effects. Fig. 5 is a photograph of a series of diffractometer charts which were taken from Silmanal sheets aged at different temperatures. In the angle range between (111) and (200) of the Ag phase at approximately 39.4° and 44.3° for 2θ respectively the change in the relative intensities of the strongest line of the β -Mn phase and of the ζ -phase with the aging temperature is shown. The respective

angle positions at approximately 42° for the (221) β -Mn and 41° for the (111) ζ are not recorded with high accuracy. As it was mentioned before an angle shift of the reflections of β -Mn was not detected up to 240°C by the more accurate film measurements. The charts, on the other hand, show more clearly than the films the increase of the amount of ζ -phase, still absent in the quenched state, in the interval between 200°C and 220°C at which temperature the reflection has gained its maximum sharpness. It broadens again at 240°C and is lost in the background scattering at still higher temperatures. An almost reversed intensity sequence of the β -Mn reflection accompanies the intensity change of the ζ -reflection. (221) reflection of β -Mn present in the quenched state, becomes weaker when the (111) reflection of the ζ -phase gains intensity, and grows stronger again above 240°C when the reflection of ζ -phase disappears.

Chemical Treatment of Silmanal Sheets

Attempts were made to separate the precipitate from the matrix in sheets which had been aged to the temperature of maximum precipitation. Three different chemical methods were used.

a) Electrochemical Method

The specimen was placed as anode in a Bollmann's electrothinning apparatus. Experiments were carried out with two different electrolytes, a 10% solution of 20g KCN + 1g KOH and a 10% solution of 5g KCN + 5g $(\text{NH}_4)_2(\text{SO}_4)_2$. The residue of the specimen was collected

on a filter paper, washed several times with distilled water and dried.

For both electrolytic solutions the residue gave low-contrast x-ray patterns that were not essentially different from the patterns of the untreated sheets, except that the intensities of the Ag lines relative to the ζ -phase lines were much lower and β -Mn had disappeared.

b) Analgamation of the Ag Matrix with Mercury

A Silmanal wire specimen was cleaned with emery paper and then immersed in mercury for three hours. The Debye-Scherrer film taken from this sample after cleaning in dilute HNO_3 is shown in Fig. 6 (b) and compared with the film of the specimen before the chemical treatment, Fig. 6 (a). The Ag lines of the lower photograph are extremely broad, the α_1/α_2 components are fused and the (333) of Ag submerged in the background. More lines of the ζ -phase became recognizable. The estimated intensities and interplanar spacing of the film are given in Table 6A. Comparing with Table 6 it is obvious that the abundance of the ζ -phase relative to the β -Mn phase is increased, resulting in four additional lines. Apparently, the preferential attack of mercury on silver enhanced the exposure of ζ -phase. Unfortunately the quality of Ag lines did not allow conclusions as to a change in the lattice constant of the Ag-mixed crystal.

c) Surface Etching with a 10% Solution of Equal Amounts of Potassium Cyanide and Ammoniumpersulphate

Silmanal wires were immersed in the above mentioned solution for two hours. In this case a greenish-white surface coating was obtained. The amount was too small to be scraped off and the wire was x-rayed with the coating. Surprisingly, the coating gave almost completely the pattern which had been obtained by Hall (25) as the electron diffraction pattern of the carbon replica of a Silmanal sample etched in the same solution as in the present work and which Hall claimed to be the pattern of the hexagonal ferromagnetic constituent. The x-ray pattern obtained in the present work is given in Table 9. The d-values and tentative indexing of Hall's electron diffraction pattern are also shown. Relative intensities are not given by Hall. Six of Hall's nine reflections are matched very well by reflections of the etching products. In addition, the strongest β -Mn line, the complete Al pattern and three unidentified lines were present on the x-ray film. The Al pattern referred to a lattice constant of 4.052 \AA , as compared with 4.049 \AA for pure Al.

The result of this experiment was not reproducible. When the etching was repeated the specimens were usually covered with a dark film which gave various x-ray patterns but different from that of Hall or, alternatively, no pattern at all but only one or two broad and indistinct low angle reflections.

Silmanal sheets subjected to the same chemical treatment over a period of three hours followed by rinsing in distilled water and drying were used as diffractometer specimens. The results confirmed convincingly the conclusions which had been drawn from the outcome of other experiments in the course of this work. The predominant phase in the etched Silmanal sheet was the ζ -phase represented with higher peak intensities than ever before obtained in Silmanal. Fig. 7 is the photograph of the diffractometer charts taken from a sheet specimen before and after etching. Before etching only the strongest line of ζ and β -Mn are present besides those of the Ag mixed crystal. After etching the intensities of the latter are greatly reduced, the β -Mn peak is hardly recognizable and the ζ -phase is represented by the complete pattern which was given in Table 3 as the pattern of ζ -phase in the binary $Mn_{1.25}Al$ alloy. This result was reproducible with the sheet etched under identical conditions.

There is little doubt that the deposits on the wire specimens are intermediate reaction products, probably complex Ag-cyanides with one or both of the other metals. Since deposits of different colour and different crystal structure were obtained, the sequence of the reactions and the speed with which the reaction products were carried off were probably different in different experiments. Most likely these differences are in connection with the surface conditions in the thinned wire. The preceding thinning in nitric acid certainly produced a state of high surface disorder, the degree of which could

be quite different in different specimens. The thinning probably changed also the microstructure by partial removal of the rolling texture from the surface and this process might also have advanced to different degrees, producing different conditions for the attack of the cyanide solution in different specimens. On the other hand the deformation texture was still fully preserved in the sheet specimens and the interface between matrix and precipitates was always in the same positions relative to the rolling plane which would be the (110) plane in f.c.c. Ag. Usually dislocations occur at the interface and the attack of the etching agent will be primarily directed towards the dislocations. If then the Ag atoms are preferentially removed by the cyanide solution one might expect that a greater number of the precipitate crystallites become exposed. The x-ray intensities of the precipitate would then increase, not only because its relative abundance increases, but also because the absorption of the diffracted radiation decreases with the removal of heavy Ag atoms from the surface.

Although the increased intensities of the γ -phase might be explained in this manner one has to be aware that it is an oversimplified model. The intensities of the β -Mn phase which, according to this model should also increase, become in fact weaker after etching. A preferential chemical attack on this phase, due to its lower Al concentration, as compared with the γ -phase, could be one possible reason. However, the complex equilibrium relations between the two phases might even be more complex by the participation of the Ag-Ag-phase and solution

of Ag in the β -Mn phase would also have to be considered. . This will be discussed in more detail together with the results of hardness and magnetic measurements in Section 4. At this point it should only be mentioned that in the isothermal section of 240°C the β -Mn precipitate is still on its way to breaking away from the Ag matrix, a process which is finished only at 400°C.

Differential Thermal Analysis

The only discontinuity in the thermal energy/temperature curve of quenched Silmanal specimens up to 500°C was a well reproducible broad exothermic peak with a maximum at 280°C, which is shown in Fig. 8. Considering the comparatively rapid heating rate in the thermal analyzer of 12°C/min., it is suggested that the energy release takes place at a lower temperature in equilibrium aging and is probably caused by the breaking away of the ζ -phase from the Ag matrix marked by the initial descent of the hardness curve (Fig. 9).

Hardness Measurements

The macrohardness of Silmanal samples aged at various temperatures for 168 hours is given in Table 11 and Fig. 9. Although the curve has only one maximum the change of slope at approximately 100°C indicates the beginning of a second age hardening process superimposing the first one which starts at room temperature. During age hardening the change in the mechanical characteristics of an alloy becomes evident long before the precipitate phase itself, or even before the accompanying change in the lattice parameters of the parent phase are noticeable.

Thus a first precipitation apparently begins below 100°C , probably at room temperature already. The hardening effect of this first precipitation is rather small, as can be concluded from the initial slope of the curve. Before the effect reaches a maximum a second precipitation sets in, producing the sharp rise of the curve typical for severe coherency strain. In the temperature range of the ascending part both the precipitates are probably coherent as to be judged from the weak and broad X-ray reflections. The temperature of the hardness maximum coincides with the temperature at which the reflections of the ζ -phase become sharp. One would therefore be tempted to attribute the strain release following the hardness maximum to the breaking away of the ζ -crystals. However, this will not be the only event that occurs at the overaging temperature, but a series of events will take place and the smooth slope of the descending curve does not give information about starting point and temperature range of individual steps. Formation and dissolution of the metastable ζ -precipitate, formation and grain growth of the stable β -Mn precipitate have occurred when finally, at 400°C , the latter becomes optically visible in a Widmanstätten pattern on planes of the Ag mixed crystals.

Microscopic Analysis

Micrographs of Silmanal are shown in Fig. 10. In the quenched state (Fig. 10a) the microstructure is that of a single phase. Unfortunately, samples free of etchpits could not be obtained. After

aging at 240°C , the temperature at which the crystals of both precipitates have grown sufficiently large to give reasonably sharp X-ray reflections, the microstructure is still not resolved in an optical micrograph with a magnification of 1000 X, (Fig. 10b). Neither did electron micrographs taken from carbon replicas of these specimens reveal pertinent details, (Fig. 10c). The few electron transmission micrographs which finally could be taken from very small thinned sheet areas (see reference in Section 2) were far too indistinct to show the expected strain pattern surrounding coherent precipitate clusters, (Fig. 10d). After aging at 400°C the Widmanstätten pattern reported by previous investigators, (21) and (25), was obtained (Fig. 10e). At this aging temperature the β -Mn phase was the only phase which showed up in the X-ray patterns besides the Ag mixed crystal and hence, the Widmanstätten lamellae are precipitates of the β -Mn structure type, whatever the chemical composition of this phase. Since two sets of traces of the precipitate are perpendicular it may be concluded that they are deposited on the cube planes of the Ag-mixed crystals. This relation is expressed in Table 6 by the coincidence of (310) of the β -Mn phase with the (200) of Ag.

3.3 Magnetic Properties of Silmanal

Saturation magnetization, measured at room temperature, residual magnetization and coercive force of quenched and aged Silmanal samples are shown in Table 12. The data are derived from the complete hysteresis loops of the alloys, some of which are given in Fig. 11

to 14. The variation of the magnetization with temperature and time shows the gradual release of the ferromagnetic phase which is very much along the same lines that had been found for the release of the γ -phase as shown by the variation of its X-ray intensity. Only, the more detailed magnetic data give now a more quantitative picture of the time and temperature dependence of the precipitation of the γ -phase. This information is summarized in Fig. 15. The graph shows the increase of the saturation magnetization with the aging time for the two temperatures. At 200°C the magnetization has not reached its final value after 21 days. At 240°C the initial rise of the curve is much steeper and the magnetization does not change essentially after three days. Table 12 shows on the other hand that the coercive force is independent of the aging time. This is to be expected, as the coercive force is not an extensive property like the magnetization. There seems to be some influence of the quenching temperature, the higher temperature producing the higher value. There is also an influence of the magnetic field noticeable, that was applied to the specimen in one of the aging experiments. It produced the highest value of the coercive force which was measured on Silmanal in the present work. The field however had no effect on the magnetization. An effect of the field on the amount of precipitation could only be expected if it would shift the thermodynamic equilibrium between γ -phase and Ag solid solution. That is to say when with the superposition of the field energy $4\pi I \times H$ the free energy of

the system is noticeably lowered by the precipitation of the γ -phase, the temperature and amount of the phase release would be controlled by the external field. The thermodynamic data and consequently, the field energy necessary to produce an observable shift of the precipitation temperature are not known, but it would certainly have to be at least by one order of magnitude higher than that of the experimental field of 1700 Oe*. On the other hand, even a small field will have an orientating effect on the precipitating crystals and hence, will increase the coercive force when the crystals possess magneto-crystalline anisotropy. In this case, of the many possibilities which are offered for a parallel alignment of (311) planes of γ -crystals with (111) planes of the Ag mixed crystals (see Table 6) the ones are selected which provide small angles between the direction of easy magnetization and the field direction. The degree of magnetic alignment and hence, the difference between the coercive force attained with and without the external field will depend on the strength of the anisotropic field in the precipitating crystals. Since this difference is rather small in the present case it might be concluded that the magnetic anisotropy does not play an essential part in the high coercive force of Silmanal.

* A shift of the thermodynamic equilibrium temperature austenite \rightarrow martensite by 6°C was obtained by E.I. Estrin (35) with a field of 18.6 kOe. In order to produce the same field energy in the γ -phase with approximately half the saturation magnetization, $\mathcal{E} = 100$ gauss (31) against 204 gauss in low-carbon steel, the field would have to be twice as high.

The Curie temperature of Silmanal was found by repeated measurements to be 355°C as compared with 360°C given by Potter (1).

3.4 The ζ -Phase in Alloys with Small Ag Content

After the ζ -phase had been recognized as the ferromagnetic constituent in Silmanal and the coherent precipitation of this phase as the source of the high coercive force in the alloy, the program was extended to the investigation of alloys with smaller Ag content. Phase relations and magnetic properties of these alloys were expected to give additional information about the role of Ag in the magnetic properties of Silmanal.

Alloys with approximate mole fractions 0.01, 0.05, 0.1 and 0.5 of Ag, or more exact, of the formulae $\text{Ag}_{0.02}\text{Mn}_{1.11}\text{Al}_{0.89}$, $\text{Ag}_{0.1}\text{Mn}_{1.11}\text{Al}_{0.89}$, $\text{Ag}_{0.2}\text{Mn}_{1.11}\text{Al}_{0.89}$ and Ag_2MnAl were prepared in the same way as Silmanal and the homogenized and quenched samples subjected to various aging treatments. The relative abundance of the phases present in the X-ray patterns of the specimens is classified with I, II, III in Table 13. In the last column the attracting force of an Alnico magnet describes qualitatively the magnetic state of the specimens.

The following relations are recognized from the results given in Table 13.

- (1) The ζ -phase was preserved in the low-Ag alloys up to 0.1 mole fraction of Ag far beyond 250°C which is the limiting temperature

for τ in Silmanal. In $\text{Ag}_2\text{Mn}_{1.11}\text{Al}_{0.89}$ with 0.5 mole fraction of Ag, the τ -phase disappeared between 240°C and 300°C as is the case in Silmanal. With respect to the thermal stability of τ , the three low-Ag alloys fall therefore into line with the binary Mn-Al alloys and only

$\text{Ag}_2\text{Mn}_{1.11}\text{Al}_{0.89}$ resembles Silmanal.

- (ii) Free Ag was present only in the alloy with the highest Ag concentration, but was not detected in $\text{Ag}_{0.2}\text{Mn}_{1.11}\text{Al}_{0.89}$ with 9 at % Ag. Evidently, the Ag was dissolved in the β -Mn phase. This opens up the interesting question about the relation between a solid solution of Ag and Al in β -Mn and the Ag_3Al phase of the $\text{Al}_3 = \beta$ -Mn structure type. This relation will be discussed in Section 4.
- (iii) Throughout Table 13, the coordination between the relative concentration of the τ -phase in an alloy and the magnetic state of the alloy is evident. Like Silmanal, the $\text{Ag}_2\text{Mn}_{1.11}\text{Al}_{0.89}$ alloy is not magnetic after quenching, whereas the low-Ag alloys and the binary Mn-Al alloys are (cf. Table I), due to the absence or presence of τ in the quenched state.
- (iv) The h-phase which was not traced in Silmanal was not traced in $\text{Ag}_2\text{Mn}_{1.11}\text{Al}_{0.89}$ also. Although small amounts might not have been detected because of overlapping Ag reflections, it is rather unlikely that the phase is preserved in the

heat treatment which was applied to the alloys with higher Ag concentration. In the latter the homogenizing temperature was kept well below the stability range of the h-phase, which is given with 870°C by Kono (31).

The three phases in the low-Ag alloys are shown in the optical micrographs of Fig. 16b and 16c. Fig. 16d is the electron micrograph of the colloidal magnetite replica of one of the alloys. It shows the distribution of the ferromagnetic phase over the specimen surface in clusters which have grown to various sizes.

Results of microprobe analysis carried out on $\text{Ag}_{0.2}\text{Mn}_{1.111}\text{Al}_{0.89}$ specimens are pictured in Fig 17. The specimen current image of Fig. 17a shows dark Ag-rich inclusions in a light Mn-rich background. Fig. 17b and 17c represent specimen current images of other areas on which are superimposed an Ag X-ray line scan with high intensities displayed in the dark areas and an Mn X-ray line scan displaying low intensities in the dark areas. X-ray counting rates for Ag, Mn and Al were quantitatively recorded while scanning over light and dark areas. Using pure metal specimens as standards the following average compositions, in at. %, were calculated from the counts:

	Ag	Mn	Al
light phase	1.06	49.4	49.5
dark phase	65.4	9.7	25.0

In areas remote from the grain boundaries the deviations from the average values were not more and in general less than ± 5 in 100.

Apparently the light areas represent the two binary Mn-Al phases, η and ζ , the specimen current images of which will be indistinguishable. The Ag-rich dark phase therefore must be the phase with the β -Mn structure. From the results given in Table 13 it was concluded previously that Ag is one constituent of the β -Mn phase. From the result of the microprobe analysis one had to conclude that Ag is the main constituent of that phase, the composition of which $(\text{Ag}, \text{Mn})_3\text{Al}$ is that of the Ag_3Al phase of the β -Mn structure type with Mn in substitutional solid solution.

This result is rather unexpected. As to the reliability of the microprobe analysis it should be mentioned here, that the chemical analysis of Silmanal aged at 240°C , in which state the fine precipitate could not be resolved by the micro beam, and where therefore the analysis was a gross analysis of the total composition, the result could be checked by wet analysis. They were surprisingly good for a ternary system. One should therefore assume that in $\text{Ag}_{0.2}\text{Mn}_{1.11}\text{Al}_{0.89}$ too the analyzed composition of β -Mn is close to the actual composition. Yet it is difficult to reconcile this result with the experimental lattice constant. According to Pearson (loc. cit.) β - Ag_3Al has a lattice parameter of 6.934 \AA . The experimental value of 6.427 \AA , although greater than that of pure β -Mn, is of course much too small. Although extensive solid solution of Mn in Ag_3Al is possible a drastic change of the lattice constant

with the Mn concentration is not to be expected, by comparison with the Mn-Ag system, where 40 at % Mn lower the Ag parameter by less than 0.2%. Recommendations for further investigation of the problems connected with the β -Mn phase will be given in Section 4.

Magnetic data on low-Ag alloys are given in Table 14 and hysteresis loops in Figs. 18 and 19. The last alloy in Table 14, belonging to another system will be dealt with later.

Magnetic specimens of the $\text{Ag}_{0.2}\text{Mn}_{1.11}\text{Al}_{0.89}$ alloy could not be prepared by machining to proper size, as the alloy, like the binary Mn-Al alloys, was too brittle. Therefore the specimens were cast in appropriate molds. Fig. 18a is a hysteresis loop of a specimen as cast, Fig. 18b was taken after the specimen was aged at 300°C .

Comparing the magnetic data of the low-Ag alloys with that of Silmanal given in Table 12, one readily realizes that the low-Ag alloys exhibit a remarkably high value of the coercive force, although they remain considerably below the Silmanal values. The greater thermal stability of the γ -phase in the $\text{Ag}_{0.2}\text{Mn}_{1.11}\text{Al}_{0.89}$ alloy, as compared with the alloy with 1/2 mole fraction of Ag and with Silmanal was discussed with Table 13. It appears now that the presence of γ -phase in the cast state is already associated with the relatively high coercive force which does not undergo substantial change during aging. On the other hand, the heat treatment had a pronounced effect on the magnetization, raising this property to an amount which was obtained in Silmanal only after long-time aging at

200°C. Relatively lower magnetization was measured in the $\text{Ag}_2\text{Mn}_{1.11}\text{Al}_{0.89}$ alloy. Since the saturation magnetization is proportional to the relative amount of the ferromagnetic phase it follows that in $\text{Ag}_2\text{Mn}_{1.11}\text{Al}_{0.89}$ the same amount of τ -phase was produced on aging at 240°C as in Silmanal on aging at 200°C over equal time periods.

The Curie temperatures of the alloys discussed so far are compiled in Table 14. Three other alloys are included in the table. They will be discussed in Section 3.5.

The value obtained for the binary Mn-Al alloy is the same as quoted by Kono (31), the value obtained for Silmanal is slightly lower than given by Potter (1) with 360°C. The low saturation magnetization of $\text{Ag}_2\text{Mn}_{1.11}\text{Al}_{0.89}$ made the observation of the disappearance of the signal in the oscilloscope rather uncertain and the true Curie temperature might be a few degrees higher than 340°C. Yet it was certainly not higher than that of Silmanal as one would be inclined to expect from the decrease of θ with increasing Ag in the sequence 380°C - 377°C - 355°C.

However, the apparent dependence of θ on the Ag concentration of the alloy would be significant only if it could be interpreted as the result of an increasing Ag concentration in the τ -phase itself. This cannot be proved, as the changes in the lattice dimensions with the substitution of Al by Ag are very small and certainly below the accuracy with which the lattice parameters of the τ -phase, which does not give high angle reflections, could be measured. Yet it is very likely that the state of the Mn 3d shell will undergo some change when first order

Al neighbours are substituted by Ag. The one valency electron of Ag is likely to exhibit a strong tendency to go into the Mn 3d shell as was observed with Cu in the system Cu-Mn-Sb (16). The result would be an increase of the radius of the shell, and consequently a decrease of the Bethe-Slater ratio $\frac{\text{interatomic distances}}{\text{radius of 3d shell}}$ on which the Curie temperature depends, as was outlined in the introduction of the thesis.

To summarize the information which might be claimed as forthcoming from the experimental Curie temperatures one should say:

1. The Curie temperatures in the Ag-Mn-Al series of Table 15 differ only by a maximum of 25°C and hence indicate that they belong to one and the same phase. This fact can be regarded as the final proof that the τ -phase is the ferromagnetic constituent of Silmanal.
2. The variation of θ in this series possibly indicates an effect of Ag on the state of the Mn 3d shell, produced by a change in the average number of Ag atoms becoming first order neighbours of Mn. The variation of θ would therefore reflect the change in the amount of solid solution of Ag in the τ -phase, increasing from zero in the binary alloy to a maximum in Silmanal. It is true that the change of θ is not a monotonous function of the Ag concentration in the alloy, but one has to realize that the concentration of Ag in τ will not be proportional to its concentration in the bulk alloy because of the different mechanism of formation in low-Ag and

high-Ag alloys as previously discussed. In the former, that is in the binary alloys, and in the alloy with 0.1 mole fraction of Ag, the τ -phase forms by transformation of the h-phase. In the latter, that is in Silmanal and in the alloy with 0.5 mole fraction, τ precipitates from the supersaturated Ag mixed crystals in coherent dispersion.

3.5 The Effect of Small Addition of Cu and Ni on the Structure and Magnetic Properties of $\text{Mn}_{1.11}\text{Al}_{0.89}$

To gain additional information about the role of Ag in the stabilization of the τ -phase a study was made of alloys with small additions of other metals, instead of Ag, to $\text{Mn}_{1.11}\text{Al}_{0.89}$. The elements Cu and Ni were selected for this substitution.

Alloys of the compositions $\text{Cu}_{0.02}\text{Mn}_{1.11}\text{Al}_{0.89}$, $\text{Cu}_{0.2}\text{Mn}_{1.11}\text{Al}_{0.89}$ and $\text{Ni}_{0.2}\text{Mn}_{1.11}\text{Al}_{0.89}$ were prepared in the same way as the low-Ag alloys. They were brittle, ferromagnetic after casting, and the ferromagnetism was retained after homogenizing at, and quenching from, temperatures above 800°C . Homogenizing at 700°C destroyed the ferromagnetism, but low-temperature aging did not affect it. X-ray analysis of the magnetic specimens revealed, besides the presence of the phase with β -Mn structure, and of the hexagonal h-phase, the presence of a cubic phase of B2 structure type. The latter was recognized as identical with a phase to which reference is given in Pearson's Handbook (page 247 of ref. 2). The phase was originally quoted by H. O. Dørum (36). According to the author, it is a binary

phase of the composition MnAl, with $a_0 = 2.97 \text{ \AA}$. On slight addition of Cu, the lattice constant was found to be approximately the same in the present work. Contrary to the assumption of Dorum, the phase is not a binary phase, but is apparently stabilized by small additions of Cu or Ni.* The Curie temperatures were found to be 160° and 140°C for the alloy with Cu and Ni respectively, but due to the rather low residual magnetization of the alloys, the measurements were not very accurate. Nevertheless the Curie temperatures are markedly different from that of the ζ -phase, distinguishing this phase as of an entirely different structure type with different interatomic Mn-Mn distances. It may then be concluded that, of the three metals Ni, Cu and Ag, only the latter one has the specific effect on the ζ -phase which leads to the precipitation of this phase in a metastable state.

3.6 Replacement of Al in Silmanal by Sb

In an earlier state of the thesis it seemed of interest to investigate if other ferromagnetic Mn phases would be dissolved in Ag at high temperatures, preserved in solution on quenching and precipitated

* After the work was completed, Japanese references dealing with the discovery of a ferromagnetic phase in ternary alloys derived from MnAl were spotted. In a number of short notes (37) and two papers (38), Tsuboya and Sugihara deal with the magnetic properties of a phase which they describe as having a b.c.c. structure with a_0 varying from 2.90 to 2.98 \AA according to the composition. The authors traced the phase in MnAl alloys with small addition of Fe, Co, or Ni and Cu, and furthermore in Mn-Ca alloys.

in a similar way as the γ -phase. The MnSb phase of the $B8_1$ structure type with homogeneity range up to Mn_3Sb_2 was selected.

Ag_5MnSb was homogenized at $600^\circ C$ after casting, quenched and aged at low temperatures. In contrast to Silmanal the alloy was brittle. X-ray diffraction analysis disclosed the presence of a hexagonal phase besides the Ag mixed crystal. With $a_0 = 4.11 \text{ \AA}$ the lattice constant of the latter was considerably greater than that of the Ag-phase in Silmanal, and also much greater than that of pure Ag. A solid solution of 5 at % Sb in Ag increases the unit cell edge to 4.11 \AA (pg. 301 of reference 2) and hence at least this amount of Sb was dissolved in the main phase. As it was outlined on pg. 34 of the thesis the effect of a solid solution of Mn on the lattice parameter of Ag is only slight. It will therefore be concealed by the much more conspicuous effect of Sb. For that reason the chemical composition of the second phase is not known. Structure analysis revealed a hexagonal phase, the unit cell of which was much smaller than that of MnSb. In particular, the a_0 -axis was much smaller with 3.45 \AA against 4.139 \AA in MnSb. The c_0 -axis with 4.70 \AA was only by 7% smaller than that of MnSb with $c_0 = 5.742 \text{ \AA}$.

The microstructure of Ag_5MnSb was very different from that of Silmanal. This is shown in Fig. 20. The photomicrograph in Fig. 20a, taken from a specimen aged at $140^\circ C$ is that of a clearly separated phase, distributed along the matrix crystals in a grain boundary

network. Analogous contours are outlined by the micrograph of the magnetite colloid on the surface of the specimens in Fig. 20b, indicating that the phase is ferromagnetic. A hysteresis loop of the alloy is shown in Fig. 21, the magnetic data of which were given in the last line of Tables 14 and 15. The completely different magnetic character of the phases in the two systems Ag-Mn-Al and Ag-Mn-Sb becomes apparent. The latter has higher saturation and residual magnetization, but much lower coercive force, H_c , which however, is still remarkably high. Because of the higher magnetization the coercive force for vanishing induction B_c with 1050 Oe is higher than that of Silmanal, and higher than that of any Alnico magnet. The value was interpolated from the hysteresis loop of the alloy and more points of the curve would have to be measured to make the interpolation more accurately.

The Curie point of the Ag_5MnSb alloy was found to be $320^\circ C$ that is approximately the same as that of the binary Mn Sb with $\theta = 315^\circ C$. This would indicate that the distances between the Mn atoms occupying 000 and 001/2 sites in the $B8_1$ structure type are not greatly different in the new phase.

4. SUMMARY AND CONCLUSIONS

The pertinent results of this investigation may be evaluated from three different aspects:

- a) Contribution to the knowledge of Silmanal.
- b) New pieces of information on phase equilibria in binary and ternary alloy systems, on the crystal structure of intermetallic compounds and the effect of solid solution on the structure, on the relation between crystal structure and microstructure on the one and the magnetic properties on the other hand.
- c) Opening up of possibilities for the preparation of new permanent magnets.

The nature of the metastable phase which is the ferromagnetic constituent in Silmanal was revealed. It is essentially the binary MnAl phase of the L10 structure type with probably some Ag in solid solution. Unlike in the binary Mn-Al system where the ζ -phase is formed on cooling at 750°C in a reversible transformation from a hexagonal high-temperature polymorph, in Silmanal the phase starts to precipitate in fine dispersion from a supersaturated Ag solid solution. It becomes semicoherent and detectable by X-ray diffraction between 200 and 240°C with an orientation $(311)_{\zeta} // (111)_{Ag}$. At 260°C the ζ -phase disappears and from this temperature on the Ag-mixed crystal is in thermal equilibrium with a phase of the β -Mn structure type up to 400°C, which was the highest aging temperature investigated. The results of DTA, of hardness tests and measurements of saturation

magnetization and coercive force confirm the interpretation of the X-ray results about the ζ -phase being the ferromagnetic phase, and its precipitation on the Ag-planes in fine dispersion being the cause of the high coercive force in Silmanal. The hexagonal phase, which Hall (loc. cit.) assumed to be the ferromagnetic phase, could be obtained under similar conditions as in Hall's work and is probably a reaction product of Silmanal with a cyanide-persulfate etchant.

One feature in the phase relations in Silmanal is not completely understood, but seems essential for the difference in the thermodynamic stability of ζ -phase in Silmanal and in the binary system. This is the role which the phase of the β -Mn structure type plays in the formation and transformation of the ζ -phase. Hall (loc. cit.) did not detect this phase below 400°C, and at 400°C the ζ -phase was no longer present and the other phase, the equilibrium phase, had precipitated in Widmanstätten pattern. Hall therefore concluded that a ferromagnetic phase of unknown composition transforms to the equilibrium phase above its Curie point, and that the equilibrium phase is β -Mn. This explanation is plausible from the thermodynamic point of view and is supported by the observation on other alloys that a metastable phase first precipitates and is later exchanged by the equilibrium phase, as described by Barrett in a survey of age hardening (loc. cit. Chapter XXII). It is less plausible from the chemical point of view and in the light of the results of the present

work one must say that the reaction which leads to the disappearance of the ζ -phase and to the formation of the equilibrium phase is only the last step in a sequence of events in which ζ -phase, β -Mn phase and the Ag matrix are involved. The β -Mn phase was observed simultaneously with the first appearance of the ζ -phase at 200°C, and in fact, was traced by its strongest line in the quenched state already. That the Ag matrix is involved in the precipitation of β -Mn and ζ -phase and again, in the transformation of the latter, is deduced from the change of its lattice parameter. As to the composition of β -Mn type phase, it is certainly not pure Mn; lattice spacing and relative intensities are different from that of pure β -Mn, but also different at different state of aging. In the alloy $\text{Ag}_{0.2}\text{Mn}_{1.11}\text{Al}_{0.89}$ the composition of this phase was determined by microprobe analysis to be very close to $(\text{Ag},\text{Mn})_3\text{Al}$; the lattice constant of this phase with 6.427 Å was 7% smaller than that of isostructural β' - Ag_3Al and 2% greater than that of pure β -Mn. The lattice constant of the phase in quenched Silmanal, 6.411 Å did not change on annealing up to 240°C, but increased to 6.431 Å on aging above 240°C. This change was either brought about by solid solution, or an unstable primary precipitate was consumed together with the ζ -phase during overaging and replaced by the equilibrium phase, the composition of which is still further apart from that in the binary alloy for which $a_0 = 6.388$ Å. The occurrence of two phases, one of which is rich in Ag, could tentatively be assumed to be the cause

for the instability of the ζ -phase at 240°C . One possible interpretation might be that the formation of the equilibrium phase is initiated by the precipitation of β' - Ag_3Al simultaneously with the breaking away of the ζ -phase from the Ag-matrix, and that the precipitate then becomes stable as a reaction product of these two phases. The stable product would then be a solid solution of Mn in β' - Ag_3Al . It is not claimed that this interpretation might not be at variance with one or the other experimental observations, and in particular, it is not even known whether β' - Ag_3Al with Mn solid solution may be assumed to form a Widmanstätten pattern on Ag planes; it is known only that hexagonal Ag_2Al forms a Widmanstätten pattern on Al planes (39). It seems however, that with this interpretation, more experimental ground is covered than in previous explanations.

There is no doubt that the detailed study of the structure of the Widmanstätten pattern in its early stages and microprobe analysis of its composition and change in composition with aging would reveal at least some of the hidden relations. These investigations could not be carried out within the scope of the thesis. In spite of the still open questions, it might be claimed that in the present work it was disclosed that the unique magnetic properties of Silmanal are a consequence of thermodynamic relations between an Ag-matrix which is capable of supersaturation and age hardening, and two other phases of which the structure is known. Also known is the composition of one phase and the fact that the other phase is a ternary alloy rich in Ag. The isomorphy between the latter phase and the β -Mn phase

which is preserved on quenching seems to be an essential factor and should be taken into account in the search for other systems in which, like in Silmanal, a coherent precipitate of a ferromagnetic Mn-phase should be expected.

In other alloys of the Ag-Mn-Al system with molefractions 0.01 to 0.5 Ag phase relations either similar to those in binary MnAl or similar to those in Silmanal were found dependent on the absence or presence of a free Ag-phase. In alloys of the first case the composition of individual phases could be determined by microprobe analysis which showed a small amount of Ag in the ζ -phase and a composition of $(\text{Ag}, \text{Mn})_3\text{Al}$ for the β -Mn phase with an Ag:Mn ratio close to 7:1. The Curie temperature of the ζ -phase decreased from 380 to 355°C in the sequence: binary alloy-low Ag alloy-Silmanal. The highest coercive force in this series with 70% of that of Silmanal was measured in the alloy with the highest Ag content.

The ζ -phase is not retained by the addition of small amounts of Ni or Cu to MnAl. Instead, a ferromagnetic phase of the B2 structure type is formed which was claimed by Dørum (36) to be another polymorph of MnAl, but apparently is stabilized by these metals. Like the ζ -phase, the phase transforms to β -Mn at higher temperatures. A study of the boundary conditions for the formation of ζ in the presence of other elements and of the B2 phase in the presence of Ag might be expected to give additional information about the role of Ag in Silmanal.

Replacement of Al in Silmanal by Sb resulted in an alloy which, compared with Silmanal, has a higher I_s , B^H_C and consequently a higher energy product. The latter is assumed to become a maximum for a critical Ag concentration, and further investigation of this alloy is recommended.

Table 1. Phase relations, magnetic and mechanical conditions of $Mn_{1+X}Al$ alloys after various heat-treatment. Tetragonal ζ -phase, hexagonal h-phase

Sample No.	Composition X		Thermal condition	Treatment of x-ray specimen	Relative intensities of phases			Ferromagnetic and mechanical state
	Nominal	Analysis			strong	medium	weak	
1	0		quenched from 825°C in ice-water	powder aged for 4 hours at 300°C	-	{ β -Mn h	-	non-magnetic; friable
2	0.105	0.078	quenched from 825°C in ice-water	powder aged for 4 hours at 300°C	β -Mn	h	-	non-magnetic; friable
3	0.105		quenched from 950°C in air					magnetic; friable
	0.105		quenched from 950°C in air	magnetic fraction of sample 3	ζ	-	-	strongly magnetic
	0.105		quenched from 950°C in air	non-magnetic fraction of sample 3	β -Mn		h	non-magnetic
4	0.25	0.180	as cast	none	ζ	h	-	strongly magnetic; tough for grinding
	0.25		as cast	powder aged for 168 hours at 300°C	ζ	β -Mn	h	strongly magnetic; tough for grinding
5	0.25		quenched from 800°C in air	powder aged for 4 hours at 300°C	ζ	β -Mn	h	strongly magnetic; tough for grinding
6	0.25		quenched from 950°C in air	powder aged for 168 hours at 240°C	ζ	-	h	very strongly magnetic; very tough to grind
7	0.25		quenched from 1050°C to 325°C in air and kept 5 days at 325°C	powder aged for 24 hours at 325°C	ζ	β -Mn	h	very strongly magnetic; very tough to grind

Table 2. X-ray analysis of $Mn_{1.25}Al$ alloy quenched from $1050^{\circ}C$ to $325^{\circ}C$ in air. Aged at $325^{\circ}C$ for 120 hours. X-ray specimen stress relieved at $325^{\circ}C$ for 24 hours.

Intensity	Interplanar distances, d in Å	Phases identified	I/I_0 + + +
w	4.55	β -Mn	+
w	3.57	ζ	5.6
w	2.79	ζ	6
vs	2.19	ζ ;h	100;80
s	2.14	β -Mn	100
m	2.05	h; β -Mn	100;64
m + +	1.96	ζ	37
w	1.94	β -Mn	27
f	1.78	ζ	14.5
w	1.72	ζ ; β -Mn	3;7
w + +	1.39	ζ	17
m	1.32	ζ	33
w	1.26	β -Mn	30
w	1.19	β -Mn	20
m	1.17	ζ	69
w	1.09	ζ	84

+ Reflection not given in ASTM card

++ Broad lines

+++ Calculated intensity values are taken from ASTM card No. 1-1234 for β -Mn, ASTM card No. 11-416 for h-phase and Kono (31) for ζ -phase. The I/I_0 values of the ζ -phase given in ASTM card No. 11-520 and referred to Kono are incorrect due to erroneous standardizing

Table 3. Reflections of the $\tilde{\alpha}$ -phase in $\text{Mn}_{1.25}\text{Al}$ of Table 2 compared with that of the ferromagnetic $\text{Mn}_{1.23}\text{Al}$ phase given by Kono (31)

hkl	d_{exp} in Å	d_{Kono} in Å	I/I_{exp}	I/I_{Kono}
001	3.57	3.58	w	5.6
110	2.79	2.79	w	6
111	2.19	2.19	vs +	100
200	1.96	1.97	m	37
002	1.78	1.79	f	14.5
201	1.72	1.72	w ++	3
220	1.39	1.39	w	17
202	1.32	1.32	m	33
311	1.17	1.17	m	69
222, 113	1.09	1.095	w	84

+ Coincidence with (002) of h-phase

++ Coincidence with (321) of β -Mn phase

Table 4. Reflections of h-phase in $Mn_{1.25}Al$ of Table 2 compared with that of ASTM data card No. 11-416

hkl	d_{exp} in Å	d_{ASTM} in Å	$I/I_{0_{exp}}$	$I/I_{0_{ASTM}}$
100	2.14	2.33		80
002	2.19	2.19	vs +	80
101	2.05	2.05	m ++	100
102	1.82	1.59		50
110		1.35		50
103		1.23		50
112	1.26	1.14		50
201	1.19	1.13		20
004		1.095		50

+ Coincidence with (111) of ϵ -phase

++ Coincidence with (310) of β -Mn phase

+++ Coincidence with (101) of γ -phase

++++ Coincidence with (201) of ϵ -phase

Table 5. Reflections of β -Mn phase in $Mn_{1.25}Al$ of Table 2 compared with that of ASTM data card No. 1-1234

hkl	d_{exp} in Å	d_{ASTM} in Å	I/I_o_{exp}	I/I_o_{ASTM}
110	4.55	4.55	w	+
221	2.14	2.10	s	100
310	2.05	2.00	m ++	64
311	1.94	1.90	w	27
321	1.72	1.68	w +++	7
330		1.49		3
420		1.41		3
431	1.26	1.24	w	30
432	1.19	1.17	w	20
531		1.06		3
442		1.05		3

+ Reflection not given in ASTM card

++ Coincidence with (101) of h-phase

+++ Coincidence with (201) of α' -phase

Table 6. Analysis of a Debye-Scherrer powder pattern taken from a Silmanal alloy aged at 240°C for 168 hours. β -Mn and tetragonal phases are identified by comparison with Tables 3 and 5.

No.	Intensity visual	Interplaner distances in Å	hkl		
			Ag-matrix (cubic)	β -Mn (cubic)	τ (tetragonal)
1	vvs	2.3520	(111)		
2	w	2.191	-	-	(111)
3	w	2.137	-	(221)	
4	vs	2.0370	(200)	(310)	
5	vw	1.962	-		(200)
6	vvw	1.934	-	(311)	
7	vw	1.718	-	(321)	(201)
8	s	1.4413	(220)		
9	vvw	1.326	-		(202)
10	vw	1.259	-	(431)	
11	vs	1.2309	(311)		
12	vw	1.193	-	(432)	
13	ms	1.1780	(222)		(311)
14	vw	1.071	-		(222)
15	m	1.0212	(400)		
16 α_1	s	0.9350			
α_2	m	0.9350	(331)		
17 α_1	s	0.9118			
α_2	m	0.9117	(420)		
18 α_1	s	0.8326			
α_2	m	0.8303	(422)		
19 α_1	s	0.7852			
α_2	m	0.7865	(333)		

TABLE 6A

Interplaner distances and estimated intensities of ζ -phase and β -Mn phase in Silmanal, aged at 240°C and etched in mercury

Intensity visual	Interplaner distances in Å	h k l	
		ζ -phase	β -Mn phase
f	3.570	(001)	
f	2.778	(110)	
w	2.193*	(111)	
vw	2.144		(221)
vw	1.962	(200)	
f	1.791	(002)	
f	1.718**	(201)	(321)
f	1.386	(220)	
vvw	1.322	(202)	
f	1.259		(431)
f	1.191		(432)
m	1.178***	(311)	
w	1.095	(222)	(531)

* Coincidence with (002) of h-phase

** Coincidence with (321) of β -Mn phase

*** Coincidence with (222) of Ag

Table 7. Relative abundance of precipitated phases in Silmanal alloys, homogenized at 780°C, quenched in ice-cold water and aged at various temperatures. The relative abundance classified as I and II for major and minor constituents respectively is estimated by the intensities of the strongest reflection and number of reflections.

Aging temperature T°C	Aging time hours	Relative abundance	
		I	II
as quenched	-		β -Mn(1 v.v.f. line)
200	168	τ	β -Mn
200	500	τ	β -Mn
220	168	τ	β -Mn
240	168	τ	
		β -Mn	
240	500	τ	
		β -Mn	
250	168	τ	
		β -Mn	
260	168	β -Mn	
280	168	β -Mn	
300	168	β -Mn	
350	168	β -Mn	
400	168	β -Mn	
240 + 400	168 + 168	β -Mn	
400 + 240	168 + 168	β -Mn	

Table 8. Extrapolated lattice constant of pure Ag and of the Ag-mixed crystal in Silmanal quenched and aged at different temperatures

Heat-treatment $T^{\circ}\text{C}$	Lattice Parameter \AA
Aged at 240°C for 168 hours	4.079_6
Aged at 400°C for 168 hours	4.075_1
Aged at 400°C for 168 hours followed by 240°C for 168 hours	4.075_2
Aged at 240°C for 168 hours followed by 400°C for 168 hours	4.075_5
Pure Ag, raw material	4.086_3

Table 9. Estimated intensities and interplaner distances of a Silmanal wire specimen aged at 240°C for 168 hours and etched in 10% potassium cyanide-ammoniumpersulphate solution

Intensity	d_{exp} in Å	Al mixed crystal (h k l)	β -Mn (h k l)	Electron diffraction pattern of extract reported by Hall d in Å (h k i l)
				4.72 0001
m	2.667			2.66 10 $\bar{1}$ 0
s	2.339	(111)		2.34 0002
vw	2.140		(221)	
ms	2.025	(200)		
vw	1.981			
				1.78 10 $\bar{1}$ 2
w	1.584			1.58 11 $\bar{2}$ 0
w	1.554			
vw	1.462			
ms	1.430	(220)		
vw	1.365			1.36 10 $\bar{1}$ 3
vw	1.314			1.31 11 $\bar{2}$ 2
ms	1.222	(311)		
m	1.170	(222)		1.18 0004
				1.07 10 $\bar{1}$ 4
w	1.015	(400)		
ms	0.931	(331)		
ms	0.902	(420)		
ms	0.828	(422)		
ms	0.780	(333)		

Table 10. Estimated intensities and interplaner distances of precipitate phases observed in Silmanal strip sample aged at 240°C for 168 hours and etched in mercury for 3 hours. The reflections of Ag-matrix are not shown.

Intensity estimated	d in Å	γ -phase (h k l)	β -Mn phase (h k l)
vvw	3.570	(001)	
vw	2.778	(110)	
m	2.193	(111)	
vvw	2.144		(221)
w	1.962	(200)	
vw	1.791	(002)	
vw	1.710	(201)	(321)
vvw	1.386	(220)	
w	1.322	(202)	
vw	1.259		(431)
vw	1.191		(432)
vw	1.095	(222)	
vvw	1.067		(442)

Table 10. Saturation magnetization M_s at room temperature, residual magnetization M_r and coercive force H_c of Silmanal after various heat treatments.

Table 11. Rockwell hardness of Silmanal quenched from 780°C aged for 168 hours at different temperatures.

Quenching temperature	Aging temperature	Aging time	M_s (gauss)	M_r (gauss)	H_c (oersteds)
780	24	168	15	10	1500
780	60	168	20	15	1500
780	67.5	168	24	18	1500
780	82	168	28	22	1500
780	93	168	32	26	1500
780	92	168	35	28	1500
780	84	168	38	30	1500
780	70	168	40	32	1500

* Aged in magnetic field of 1700 Oer.

Table 12. Saturation magnetization I_s at room temperature, residual magnetization I_r and coercive force I_{H_c} of Silmanal after various heat treatments.

Quenching temperature (°C)	Aging temperature (°C)	Aging time (hrs)	I_s (gauss)	I_r (gauss)	I_{H_c} (oersted)
800	200	12	15		
800	200	24	23		
800	200	72	44		
800	200	168	53	32	4800
800	200	500	74	50	4800
800	240	168	91.5	58.5	5400
780	240	12	53		
780	240	24	80		
780	240	72	88		
780	240	168	92.8	59.5	5200
780	240	500	93	62	
780	240 ⁺	76	87	50	5600

+ Aged in magnetic field of 1700 Oe.

TABLE 13 Phase Relations in Alloys $Ag_X Mn_{1.11} Al_{0.89}$ with X = 0.02, 0.1, 0.2 and 2

Composition	Quenched from ($^{\circ}C$)	Aged at ($^{\circ}C$)	for (hrs)	Relative Abundance			Ferromagnetic state
				I	II	III	
$Ag_{0.02} Mn_{1.11} Al_{0.89}$	950	-	-	τ^*			strongly magnetic
	950	240	170	τ^{**}	-	$\left\{ \begin{array}{l} \beta-Mn \\ h \end{array} \right.$	strongly magnetic
	825	300	4	$\beta-Mn$	h	τ	magnetic
	825	300	174	τ	-	$\left\{ \begin{array}{l} \beta-Mn \\ h \end{array} \right.$	strongly magnetic
	825	500	25	$\beta-Mn$	-	τ	magnetic
$Ag_{0.1} Mn_{1.11} Al_{0.89}$	825	300	4	$\beta-Mn$	τ	h	magnetic
$Ag_{0.2} Mn_{1.11} Al_{0.89}$	chill cast	-	-	$\beta-Mn$	$\left\{ \begin{array}{l} \tau \\ h \end{array} \right.$	-	magnetic
	chill cast	400	120	$\left\{ \begin{array}{l} h \\ \beta-Mn \end{array} \right.$	τ	-	magnetic
	chill cast	500	25	$\left\{ \begin{array}{l} h \\ \beta-Mn \end{array} \right.$	-	τ	weakly magnetic
	825	300	4	$\beta-Mn$	-	$\left\{ \begin{array}{l} \tau \\ h \end{array} \right.$	weakly magnetic
	825	300	170	$\beta-Mn$	τ	h	magnetic

- continued -

TABLE 13

- continued -

Composition	Quenched from (°C)	Aged		Relative Abundance			Ferromagnetic state
		at (°C)	for (hrs)	I	II	III	
Ag ₂ Mn _{1.11} Al _{0.89}	800	-	-	Ag	***		non-magnetic
	800	240	168	Ag	β -Mn	ζ	magnetic
	800	300	168	Ag	β -Mn	-	non-magnetic

* ζ -phase represented with two broad reflections

** ζ -phase represented with six reflections

*** no reflections discernible from the background except two broad Ag lines

Table 14 Saturation magnetization I_s at room temperature, residual magnetization I_r and coercive force I_c^H of Ag-Mn-Al alloys, other than Silmanal, and of Ag_5MnSb .

Alloy	Quenching Temp ($^{\circ}C$)	Aging Temp ($^{\circ}C$)	Aging time (Hrs)	I_s (gauss)	I_r (gauss)	I_c^H (Oersted)
$Ag_{0.2}Mn_{1.11}Al_{0.89}$	Chill cast	-	-	15	12	3000
$Ag_{0.2}Mn_{1.11}Al_{0.89}$		300	100	72	45	3200
$Ag_2Mn_{1.11}Al_{0.89}$	800	240	168	54	34	3800
Ag_5MnSb	600	140	200	138	68	1800

Table 15. Curie temperatures of Ag-Mn-Al, Mn-Al and their related alloys

Composition	Heat-treatment	Curie temperature θ in $^{\circ}\text{C}$
Ag_5MnAl	quenched from 780°C then aged for 168 hours at 240°C	355
$\text{Ag}_2\text{Mn}_{1.11}\text{Al}_{0.89}$	quenched from 780°C then aged for 168 hours at 240°C	≥ 340
$\text{Ag}_{0.2}\text{Mn}_{1.11}\text{Al}_{0.89}$	cast sample aged for 100 at 300°C	377
$\text{Mn}_{1.11}\text{Al}_{0.89}$	quenched from 1050°C to 325°C then aged for 120 hours at 325°C	380
$\text{Cu}_{0.2}\text{Mn}_{1.11}\text{Al}_{0.89}$	quenched from 1050°C to 325°C then aged for 168 hours at 325°C	160
$\text{Ni}_{0.2}\text{Mn}_{1.11}\text{Al}_{0.89}$	cast	140
Ag_5MnSb	quenched from 600°C then aged for 200 hours at 140°C	320

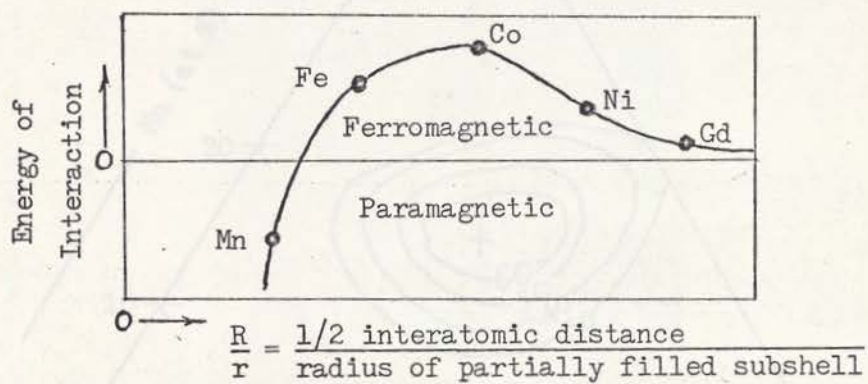


Fig. 1 Bethe's curve relating interaction energy to interatomic distance and radius of active shell

Fig. 2 Saturation magnetization M_s of $Ag-Ni$ alloy. Reproduction courtesy of *J. Appl. Phys.* of the ternary alloys (after Bethe)

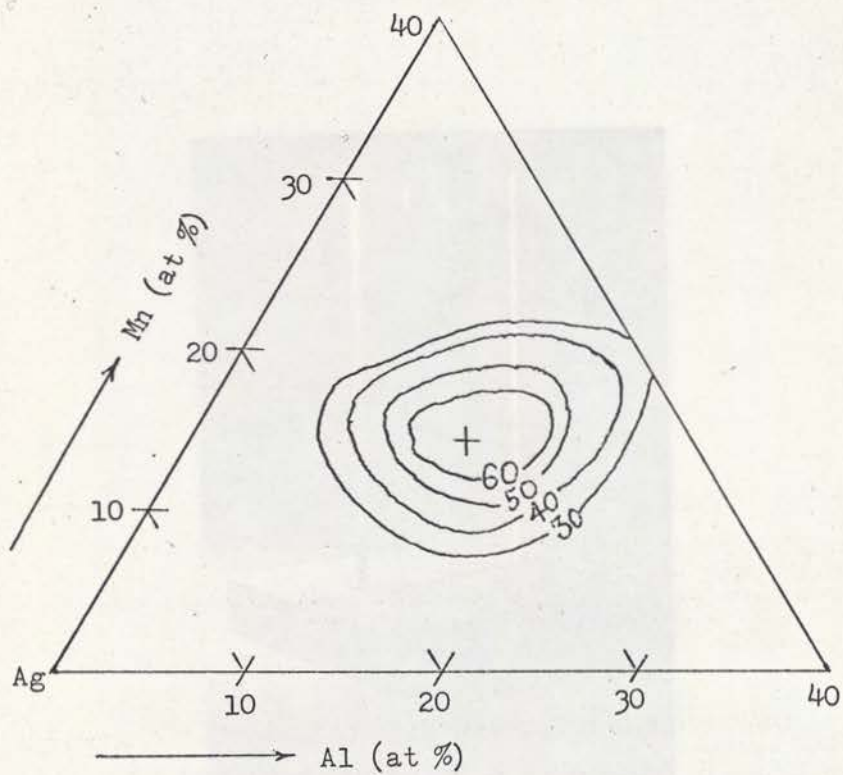


Fig. 2 Saturation intensities/cm³ of Ag-Mn-Al alloys. Magnetization contours in e.m.u./cm³ of the ternary alloys (after Potter)

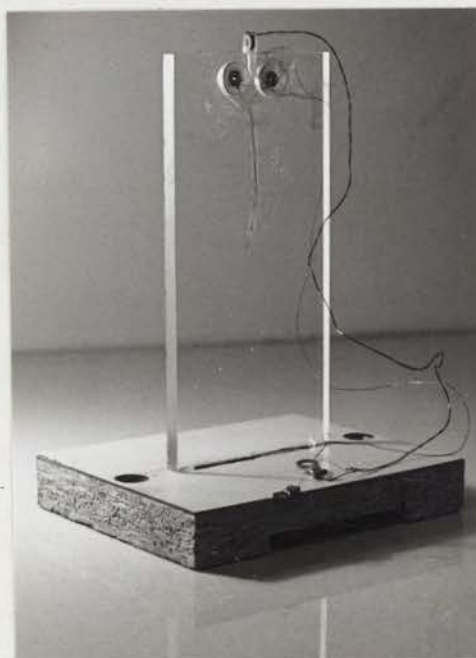


Fig. 3 (a) Holder for sample and pick-up coils
used for the magnetization measurements

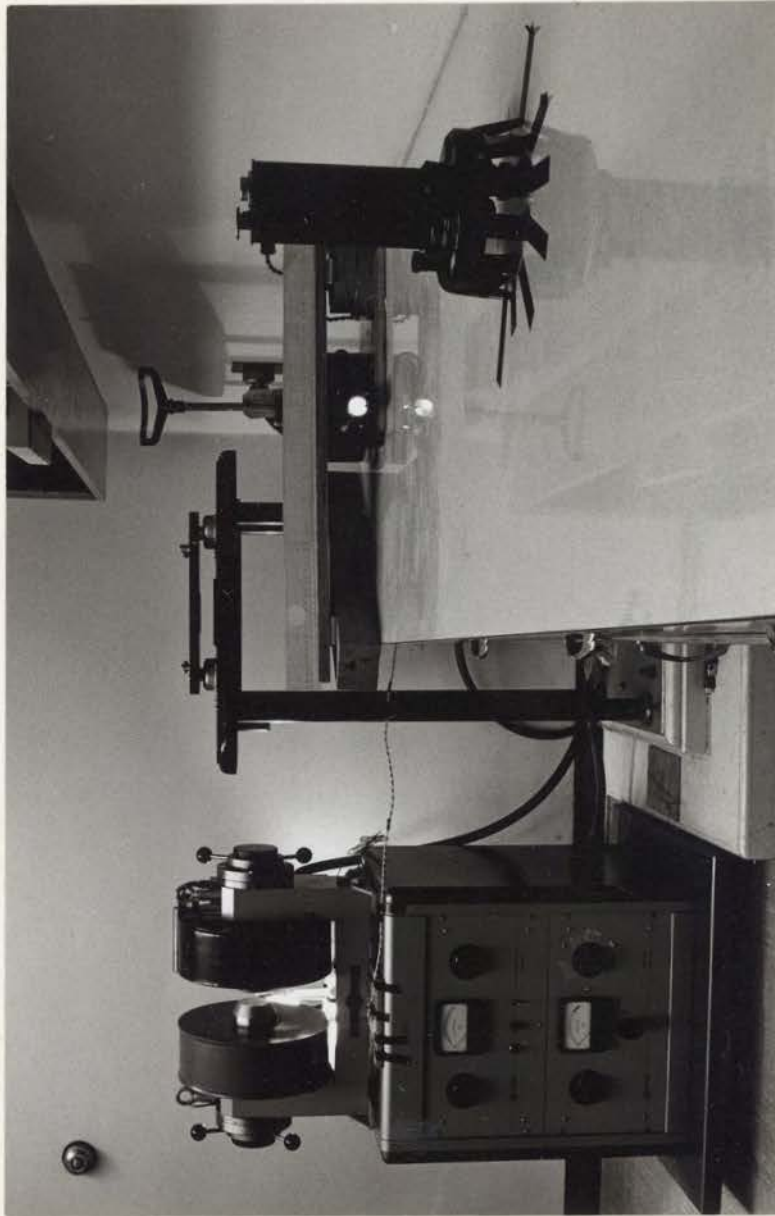


Fig. 3 (b) Magnetic measurement apparatus

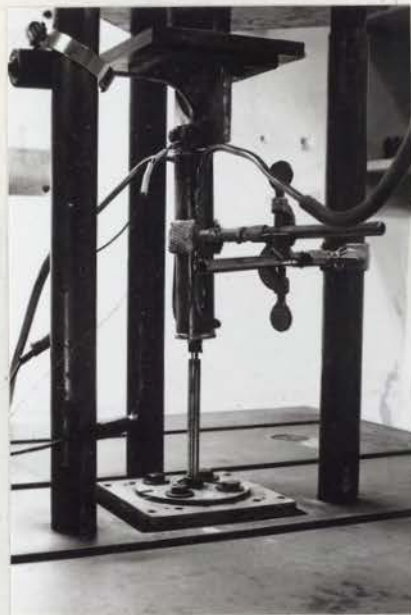


Fig. 4 (a) Sample holder for Curie
point measurements

Fig. 5 (b) Apparatus for Curie temperature
measurements

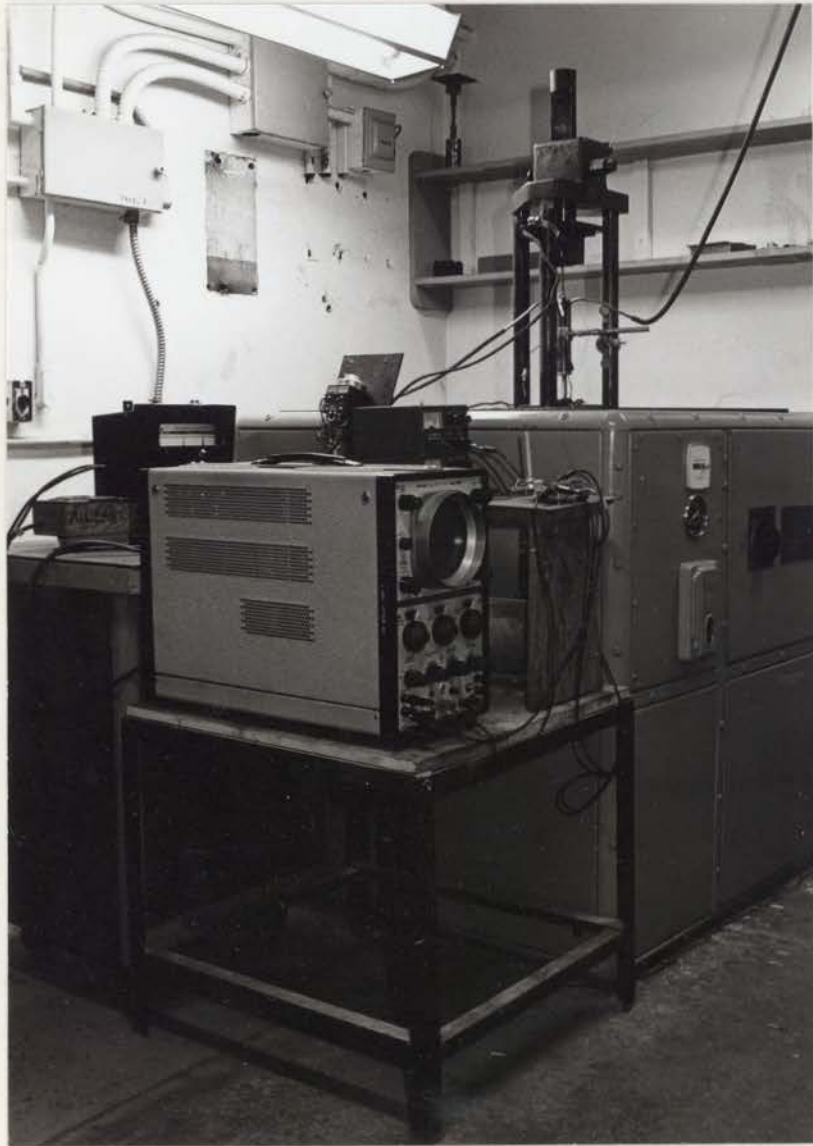


Fig. 4 (b) Apparatus for Curie temperature
measurements

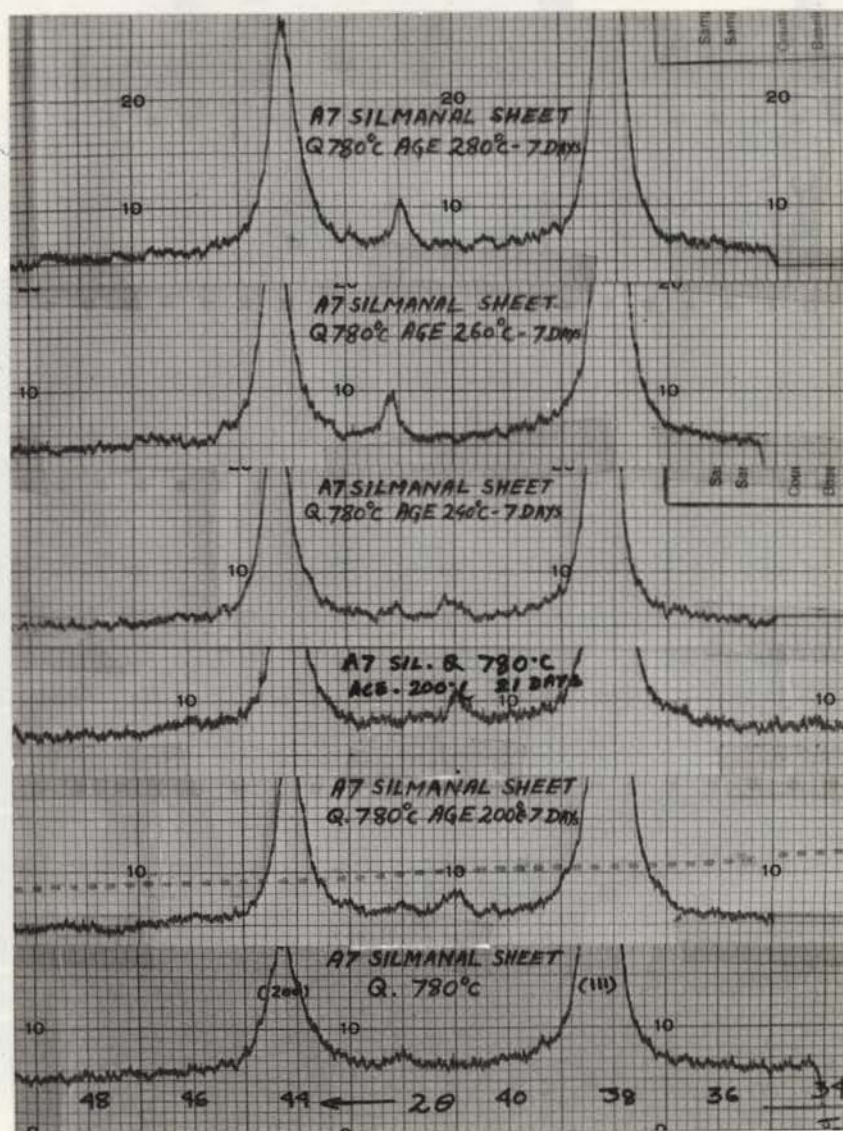


Fig. 5 Diffractometer charts of Silmanal sheets aged at different temperatures. The charts display two peaks from Ag-matrix and one peak of β -Mn (221) at $2\theta = 42.2^\circ$ and τ -phase (111) at $2\theta = 41^\circ$ only

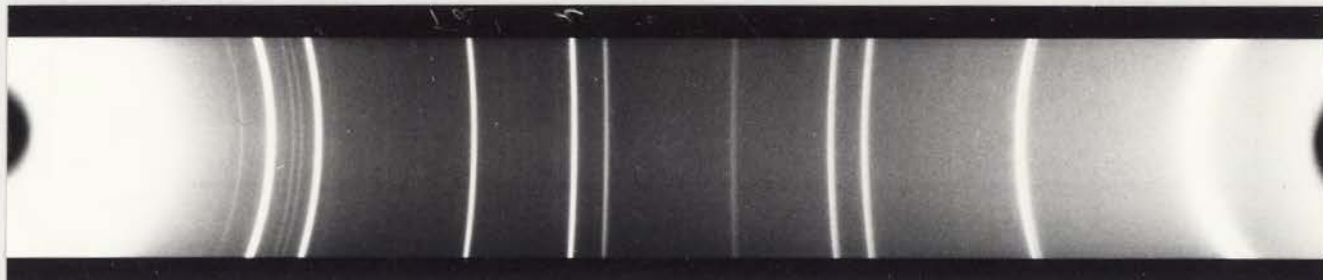


Fig. 6 (a) X-ray film from Silmanal strip sample aged at 240°C for 168 hours. Faint lines are from precipitated phases including two $\text{CuK}\beta$ lines of the (111) Ag and (200) Ag which were not completely filtered out.

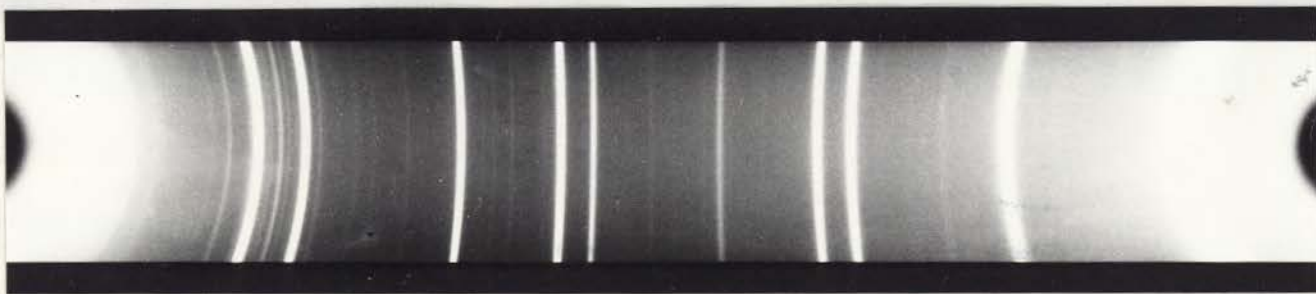


Fig. 6 (b) X-ray film from Silmanal strip sample aged at 240°C for 168 hours and etched in mercury. The faint lines additional to those in Fig. 6 (a) belong to ζ -phase.

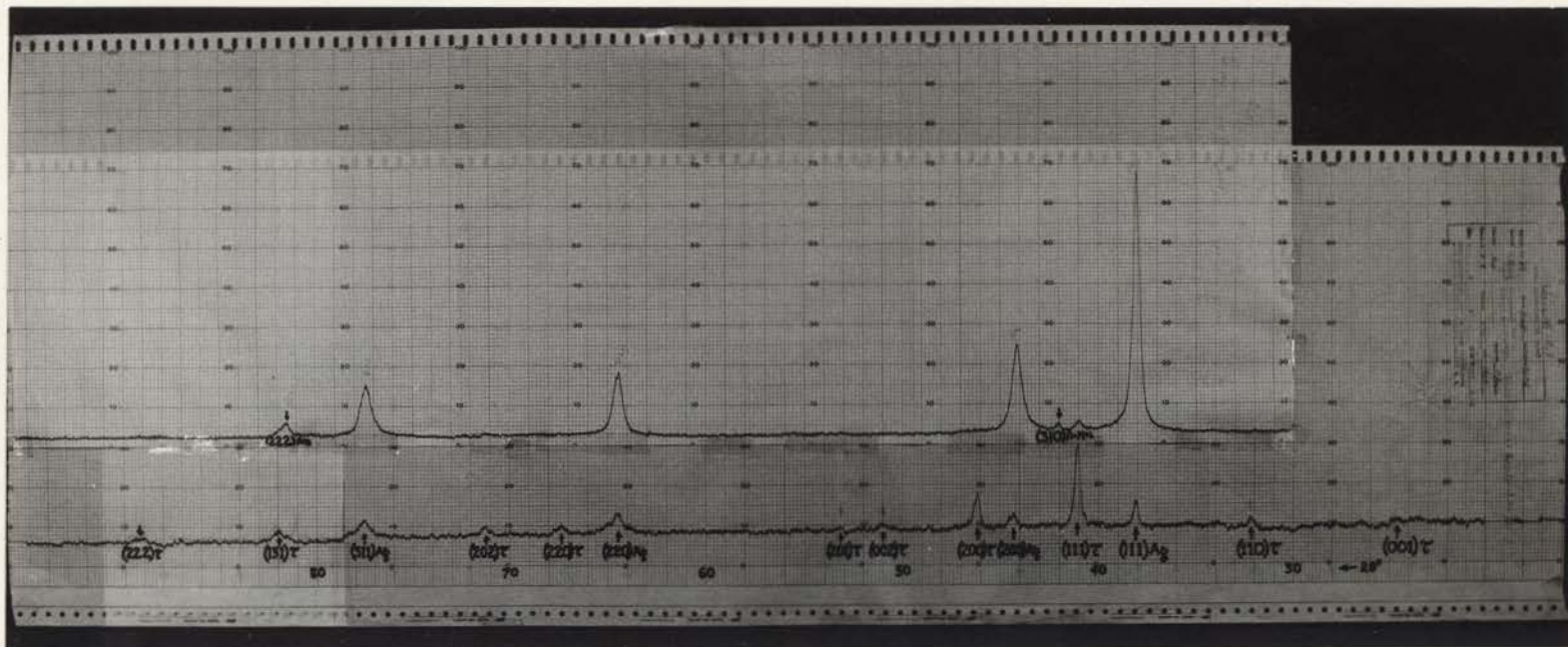


Fig. 7 Diffraction charts of Silmanal sheets aged at 240°C for 168 hours. The upper trace is that of the specimen before etching and shows besides the peaks of the Ag matrix only the strongest of the precipitated phases. The lower chart was taken after etching in 10% Potassium cyanide-ammonium persulphate solution. The ζ -phase is the predominant phase in this diffraction pattern.

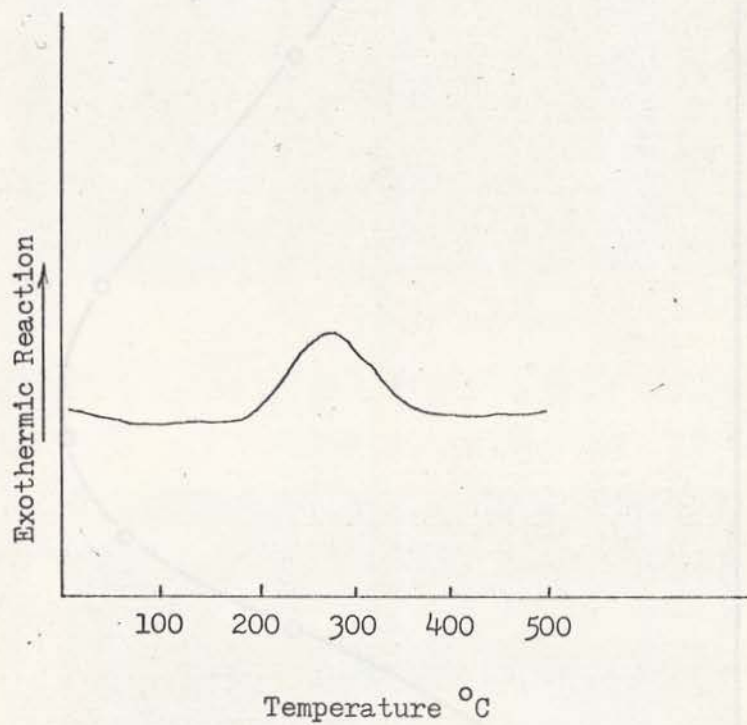


Fig. 8 Differential thermal analysis curve
of Silmanal quenched from 780°C

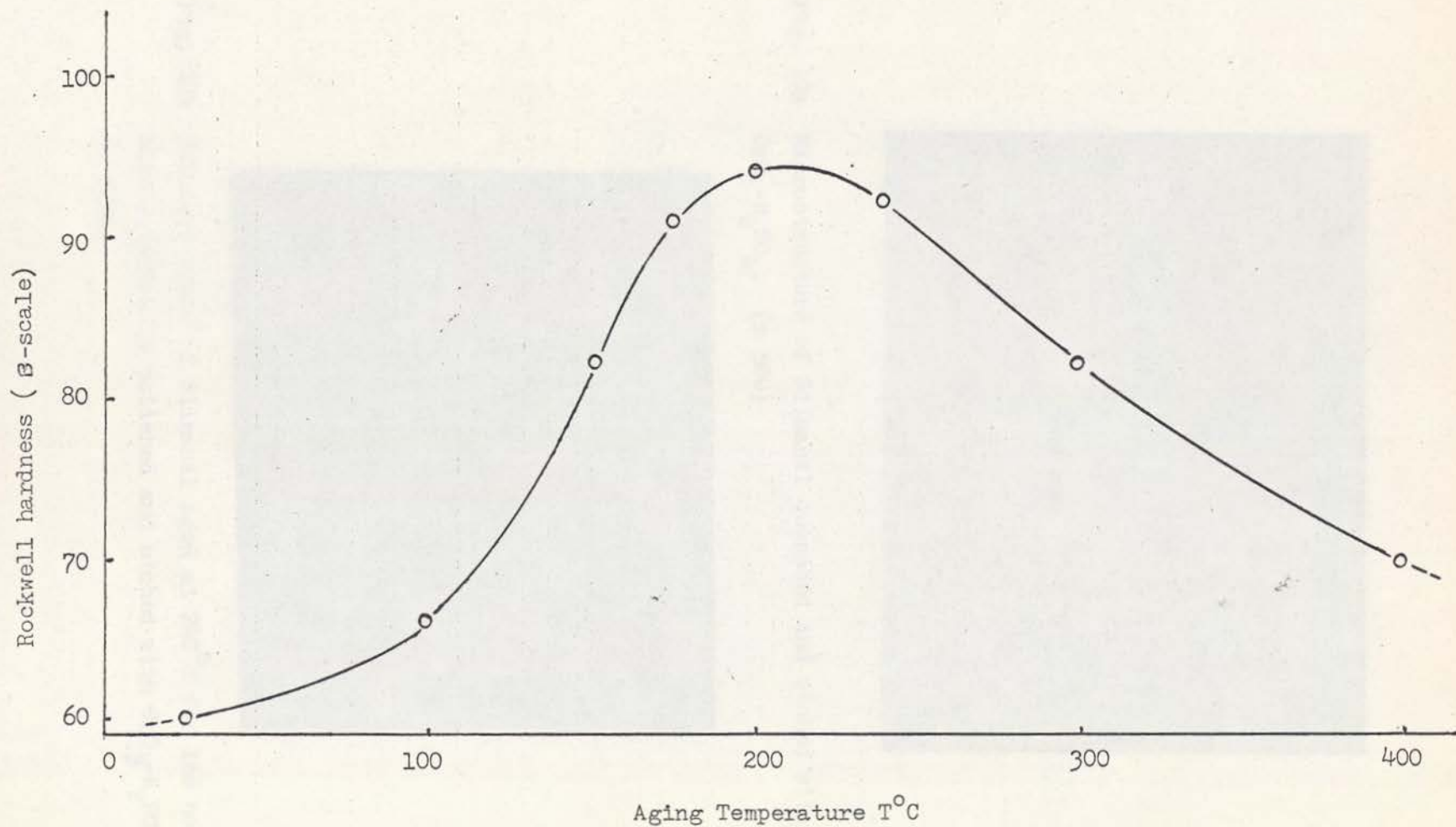


Fig. 9 Rockwell hardness of Silmanal quenched from 780°C and aged for 168 hours at different temperatures



Fig. 10a Microstructure of Silmanal quenched and etched with $\text{CrO}_3\text{-H}_2\text{SO}_4$. (x 500)



Fig. 10b Microstructure of Silmanal aged at 240°C for 168 hours. Electrolytically polished and etched with $\text{CrO}_3\text{-H}_2\text{SO}_4$. (x 1000)

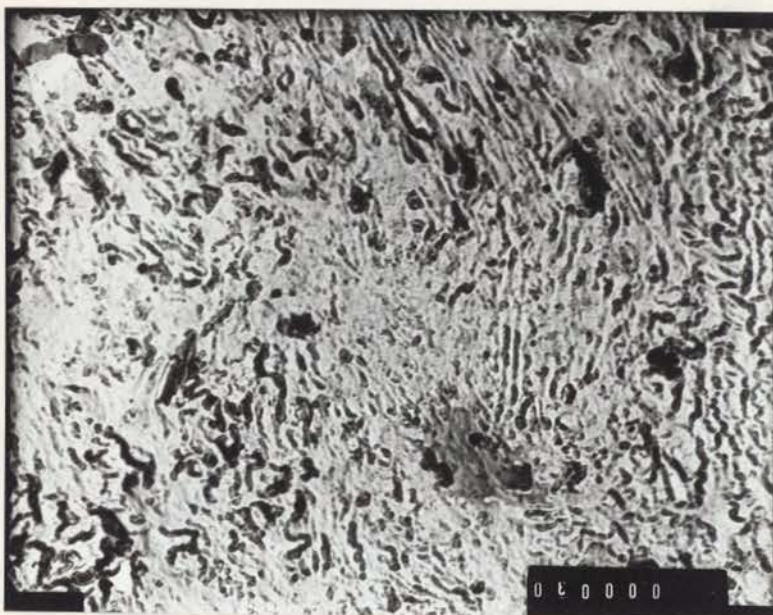


Fig. 10c Electron transmission micrograph taken from carbon replica of Silmanal aged at 240°C for 168 hours. (x 14820)

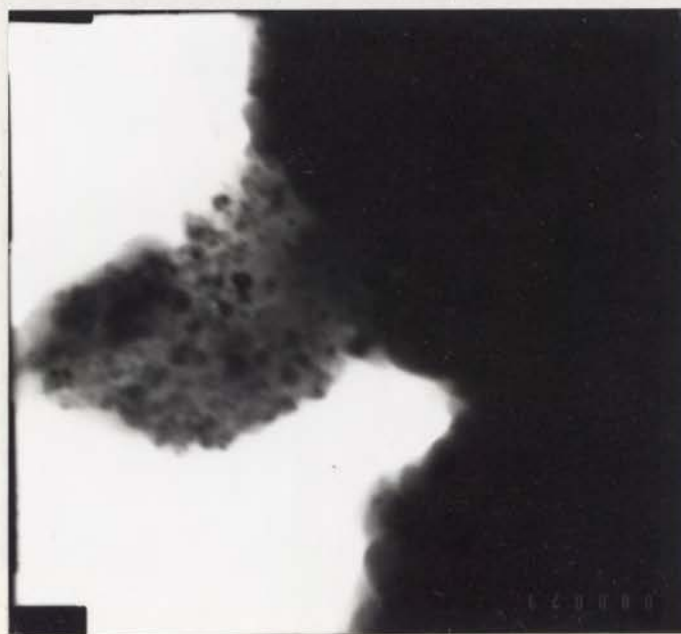


Fig. 10d Electron transmission micrograph of Silmanal aged at 240°C for 168 hours. (x 85000) Some of the dark spots are split which might be a sign of the strain pattern surrounding the coherent precipitate.



Fig. 10e Microstructure of Silmanal aged at 400°C for 168 hours, etched with $\text{CrO}_3\text{-H}_2\text{SO}_4$. Typical Widmanstätten structure (x 500)

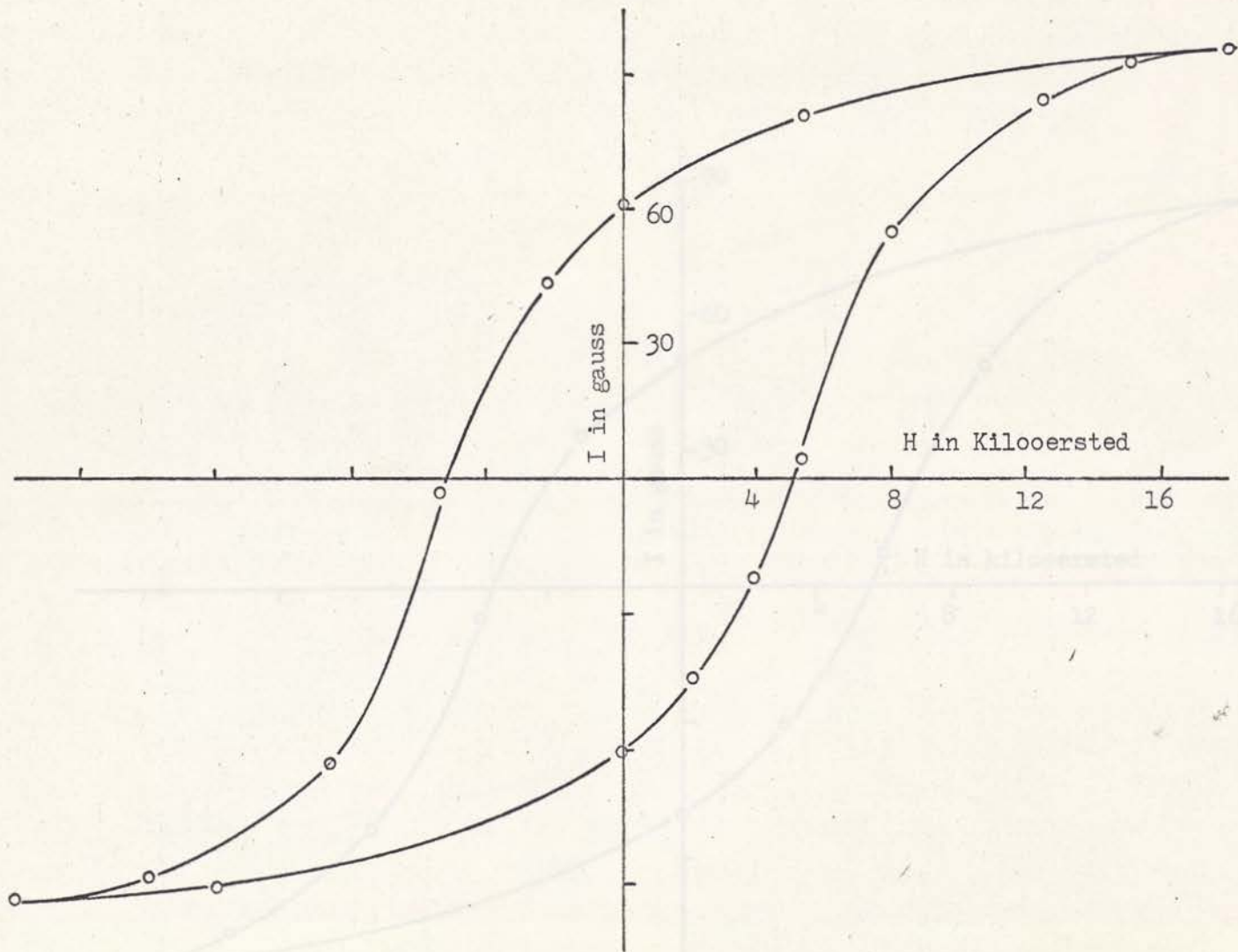


Fig. 11 Hysteresis loop of Silmanal aged for 168 hours at 240°C

Fig. 12 Hysteresis loop of Silmanal aged for 76 hours at 240°C in a magnetic field of 1700 gauss

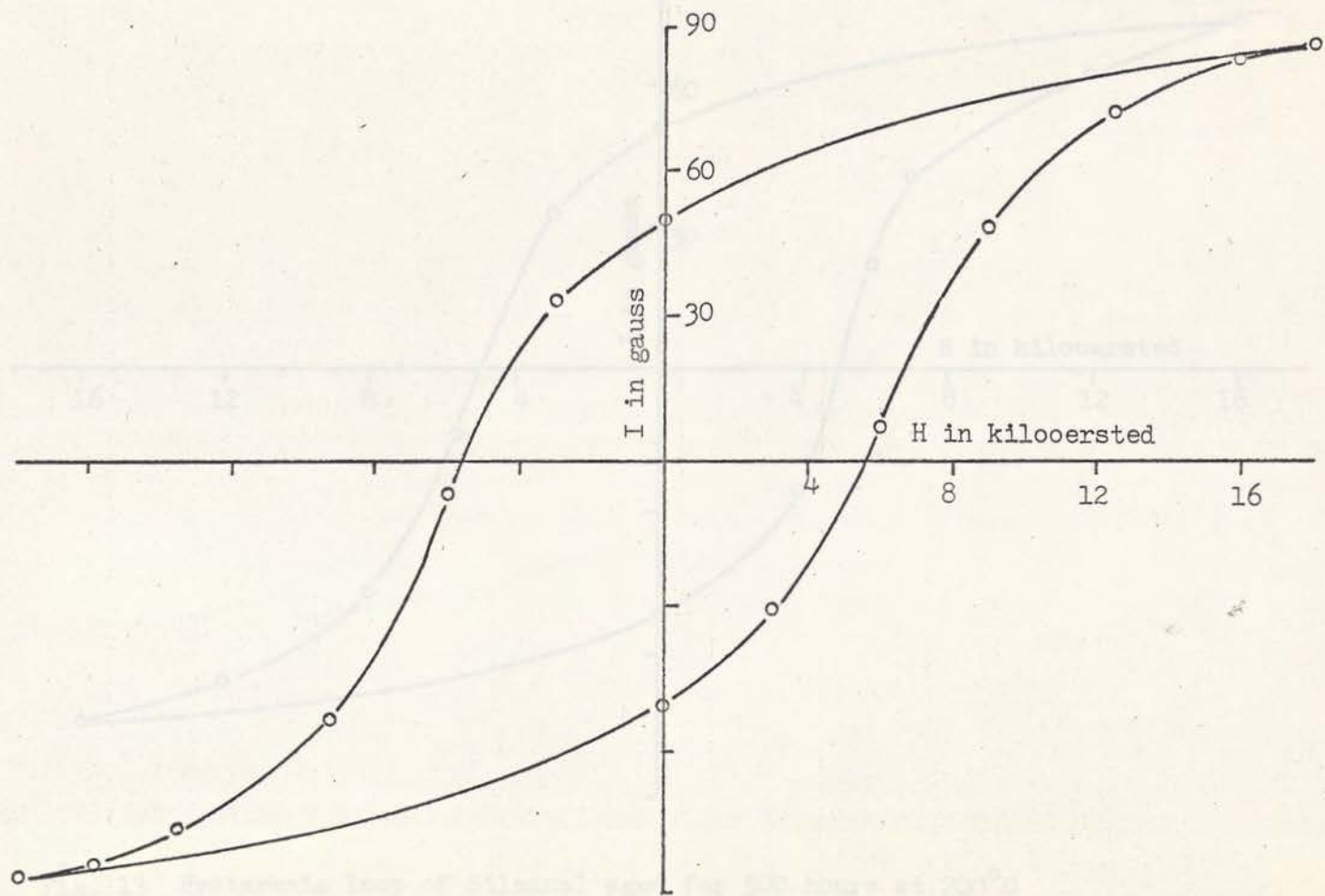


Fig. 12 Hysteresis loop of Silmanal aged for 76 hours at 240°C in a magnetic field of 1700 gauss

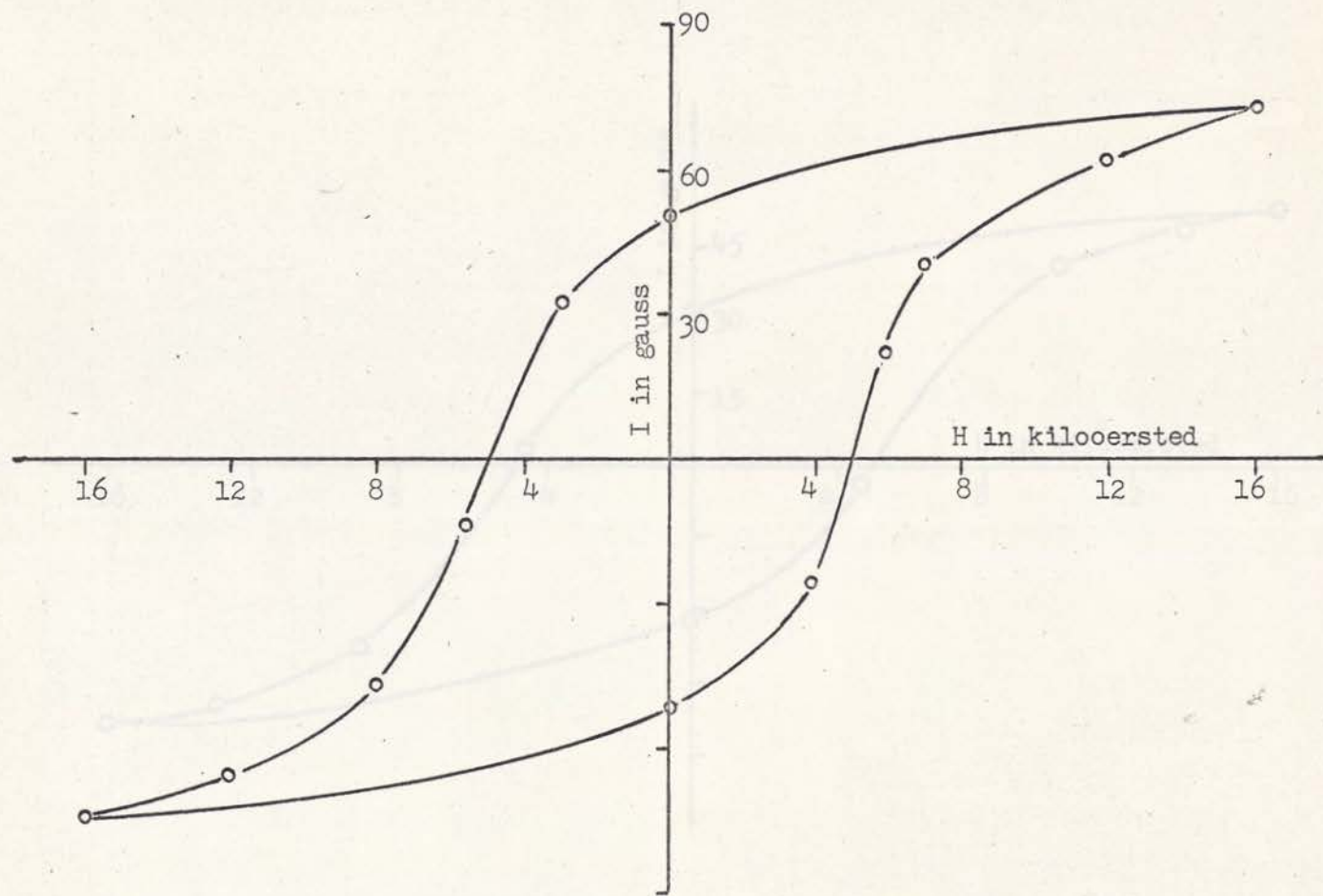


Fig. 13 Hysteresis loop of Silmanal aged for 500 hours at 200°C

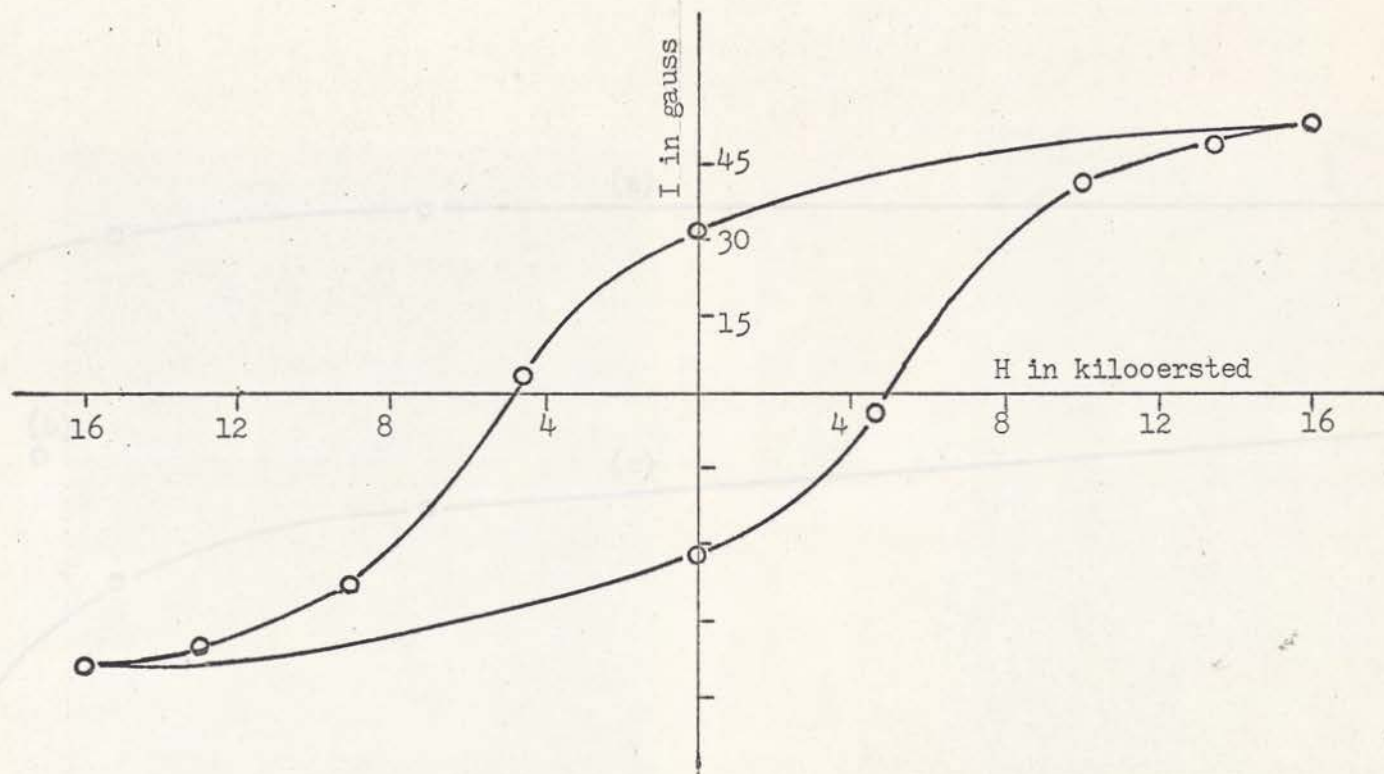


Fig. 14 Hysteresis loop of Silmanal aged for 168 hours at 200°C

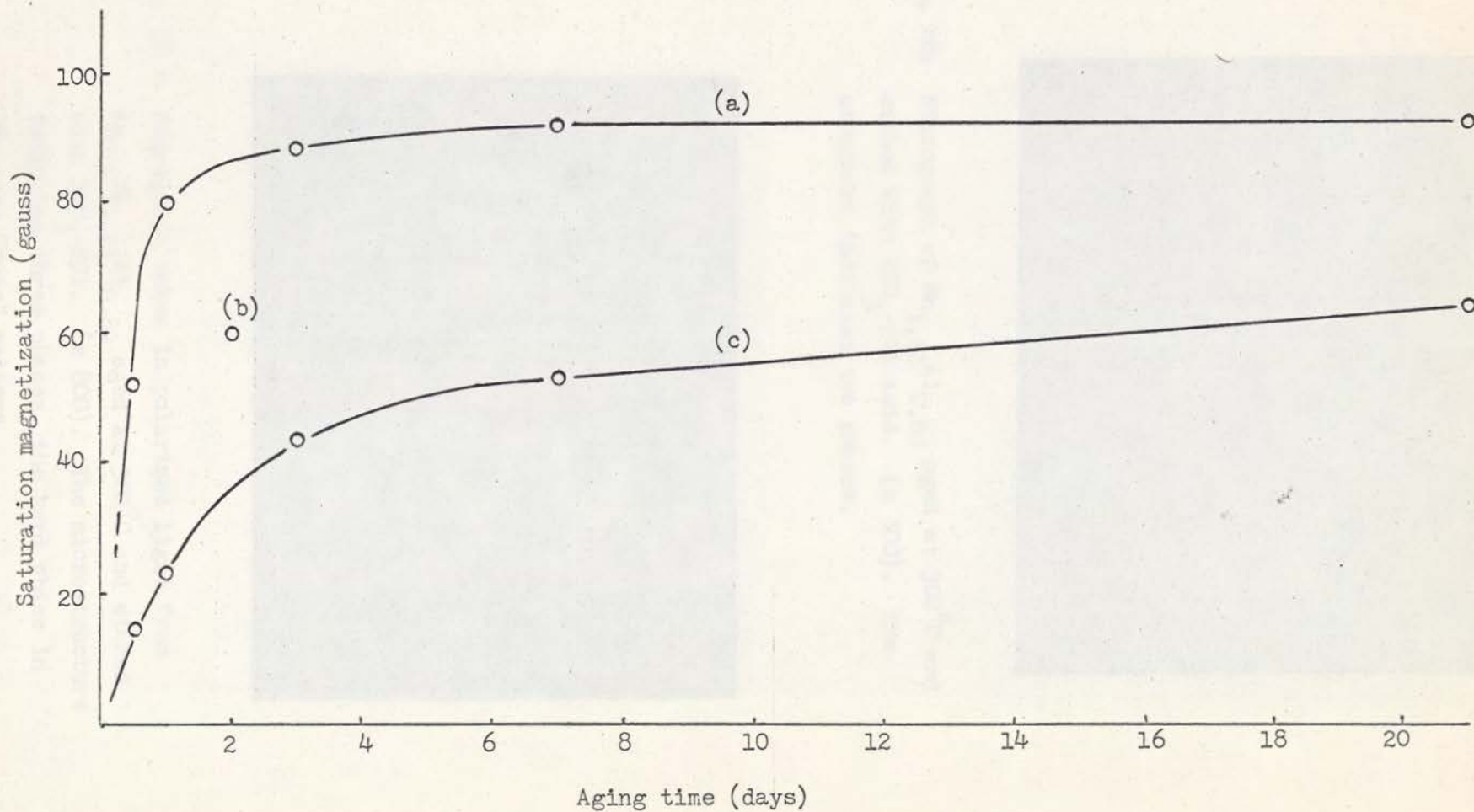


Fig. 15 Saturation magnetization of Silmanal quenched from 780°C versus aging time

- (a) Aged at 240°C
- (b) Aged at 220°C
- (c) Aged at 200°C



Fig. 16a Micrograph of $\text{Mn}_{1.11}\text{Al}_{0.89}$ aged at 300°C and etched with $\text{HNO}_3\text{-HCl}$ acid. (x 500). The structure indicates two phases.



Fig. 16 b Micrograph taken in polarized light from $\text{Ag}_{0.1}\text{Mn}_{1.11}\text{Al}_{0.89}$ aged at 300°C and etched with $\text{HNO}_3\text{-HCl}$. (x 800). The microstructure indicates three phases, the hard phase in "Maltese Cross" pattern.

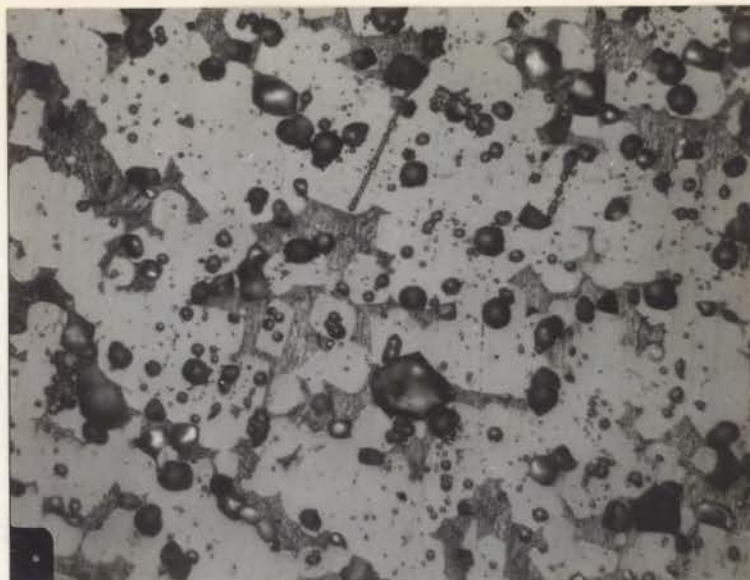


Fig. 16 c Micrograph taken in polarized light from $\text{Ag}_{0.2}\text{Mn}_{1.11}\text{Al}_{0.89}$ aged at 300°C and etched with $\text{HNO}_3\text{-HCl}$ (x 400). The microstructure indicates three phases.



Fig. 16 d Electron transmission micrograph taken from a magnetic colloid replica of $\text{Ag}_{0.2}\text{Mn}_{1.11}\text{Al}_{0.89}$ aged at 300°C . (x 14840). The replica indicates the fairly homogeneous distribution of magnetic particles in clusters grown to different sizes.

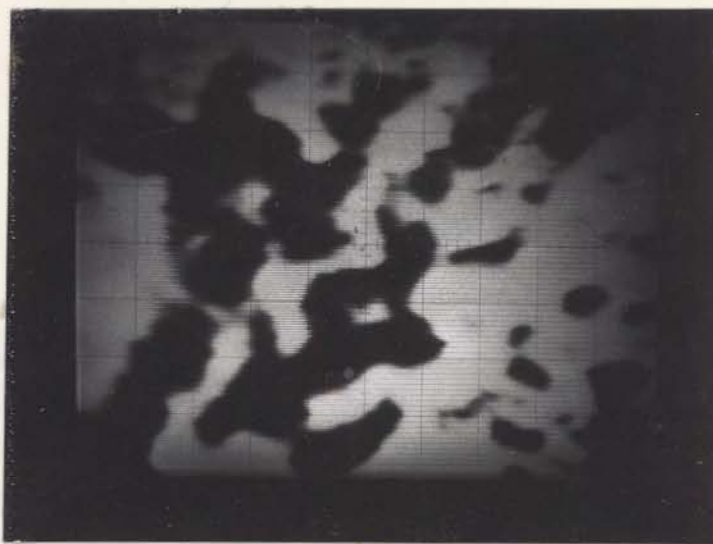


Fig. 17a Electron probe micrograph. Specimen current image of $\text{Ag}_{0.2}\text{Mn}_{1.11}\text{Al}_{0.89}$ specimen.

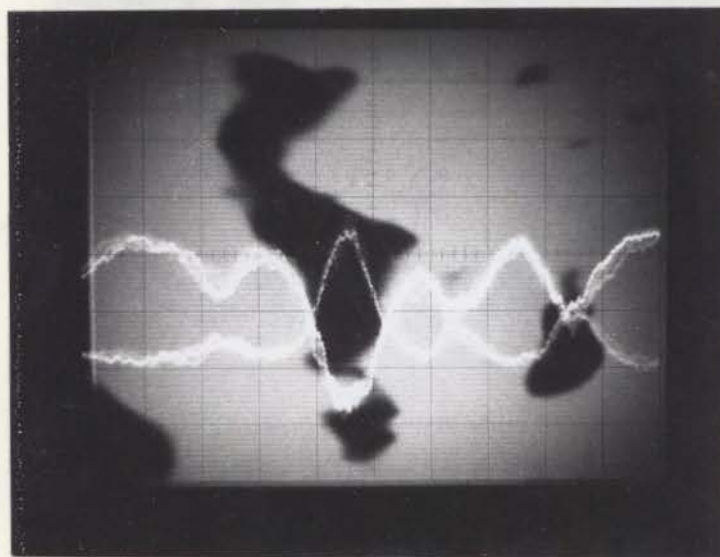


Fig. 17b Electron probe micrograph. Specimen current image with superimposed Ag X-ray scan (high intensity in dark areas) and Mn X-ray scan (low intensity in dark areas) taken from $\text{Ag}_{0.2}\text{Mn}_{1.11}\text{Al}_{0.89}$ specimen.

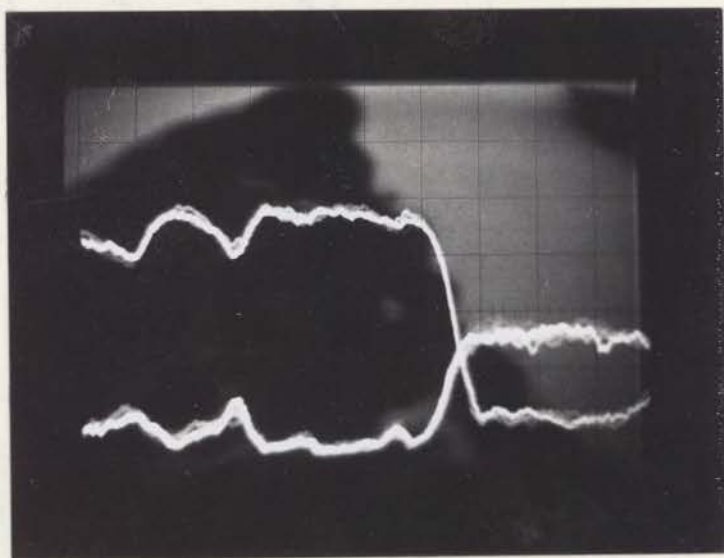


Fig. 17c Electron probe micrograph. Specimen current image with superimposed Ag X-ray scan (high intensity in dark areas) and Mn X-ray scan (low intensity in dark areas) taken from $\text{Ag}_{0.2}\text{Mn}_{1.11}\text{Al}_{0.89}$ specimen

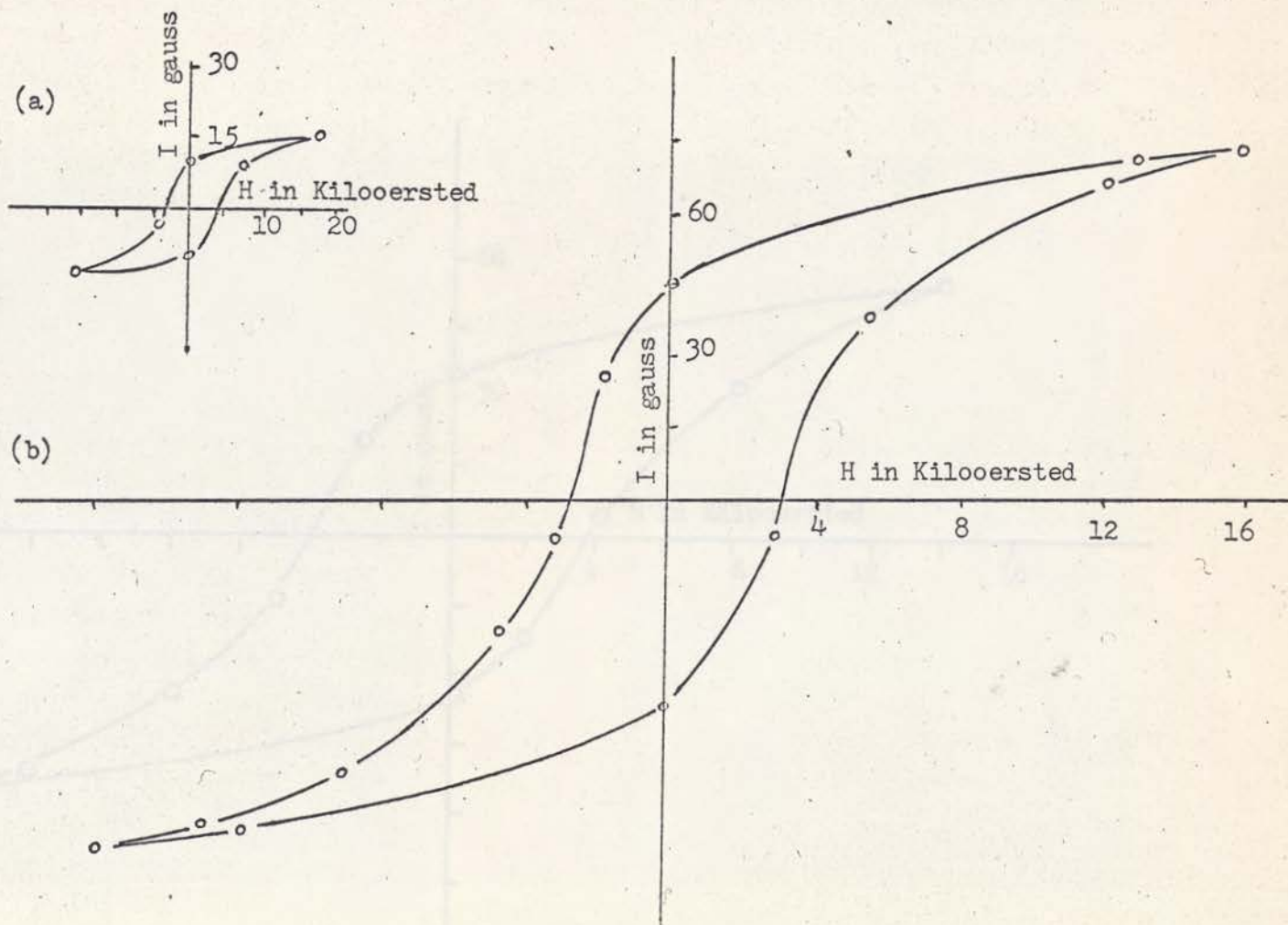


Fig. 18 (a) Hysteresis loop of cast $\text{Ag}_{0.2}\text{Mn}_{1.11}\text{Al}_{0.89}$ alloy
 (b) Hysteresis loop of cast $\text{Ag}_{0.2}\text{Mn}_{1.11}\text{Al}_{0.89}$ aged for 100 hours at 300°C

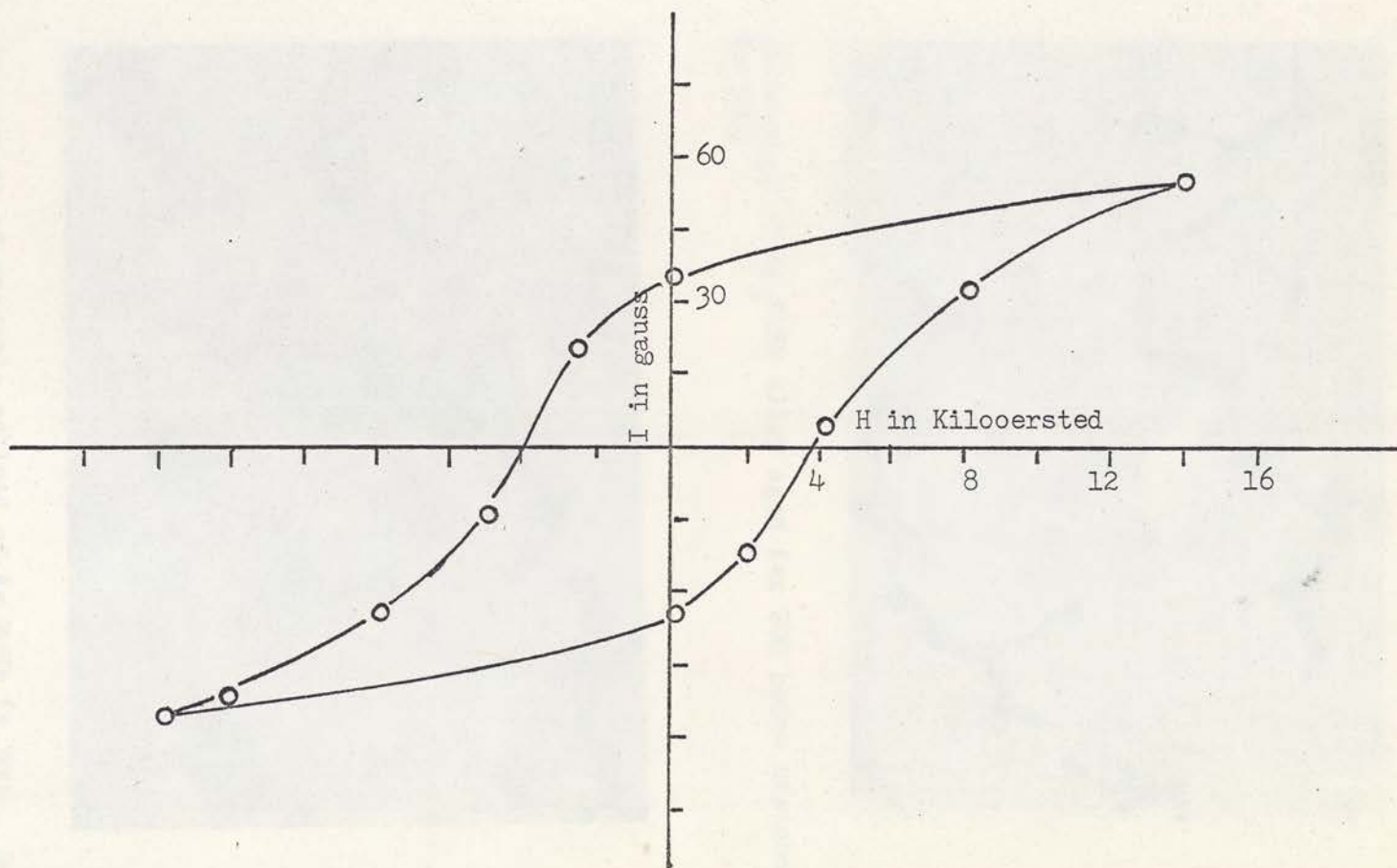


Fig. 19 Hysteresis loop of Ag₂MnAl alloy aged at 240°C for 168 hours



Fig. 20a Micrograph of Ag_5MnSb alloy aged for 200 hours unetched.
(x 500)

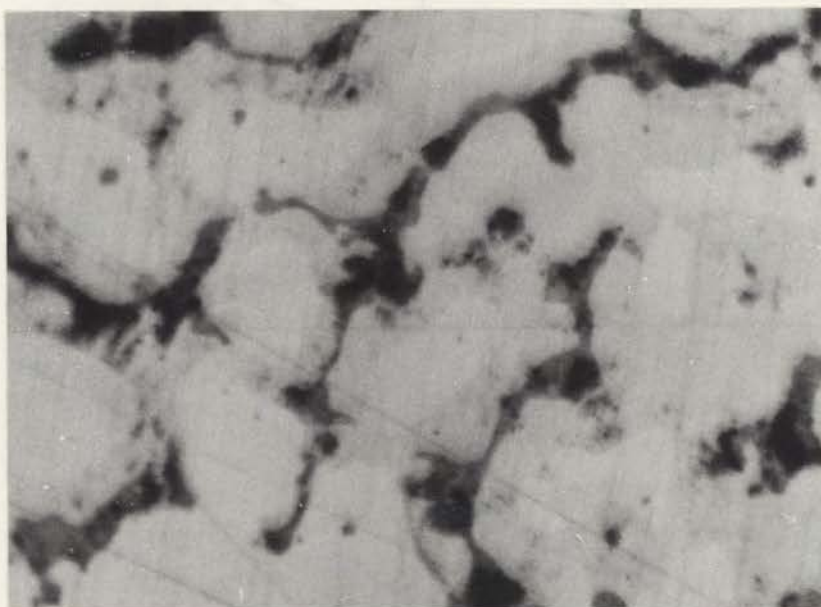


Fig. 20b Micrograph of magnetic colloid of Ag_5MnSb (x 500). By similarity of the pattern with that of Fig. 18a the dark areas in the latter are recognized as the ferromagnetic phase.

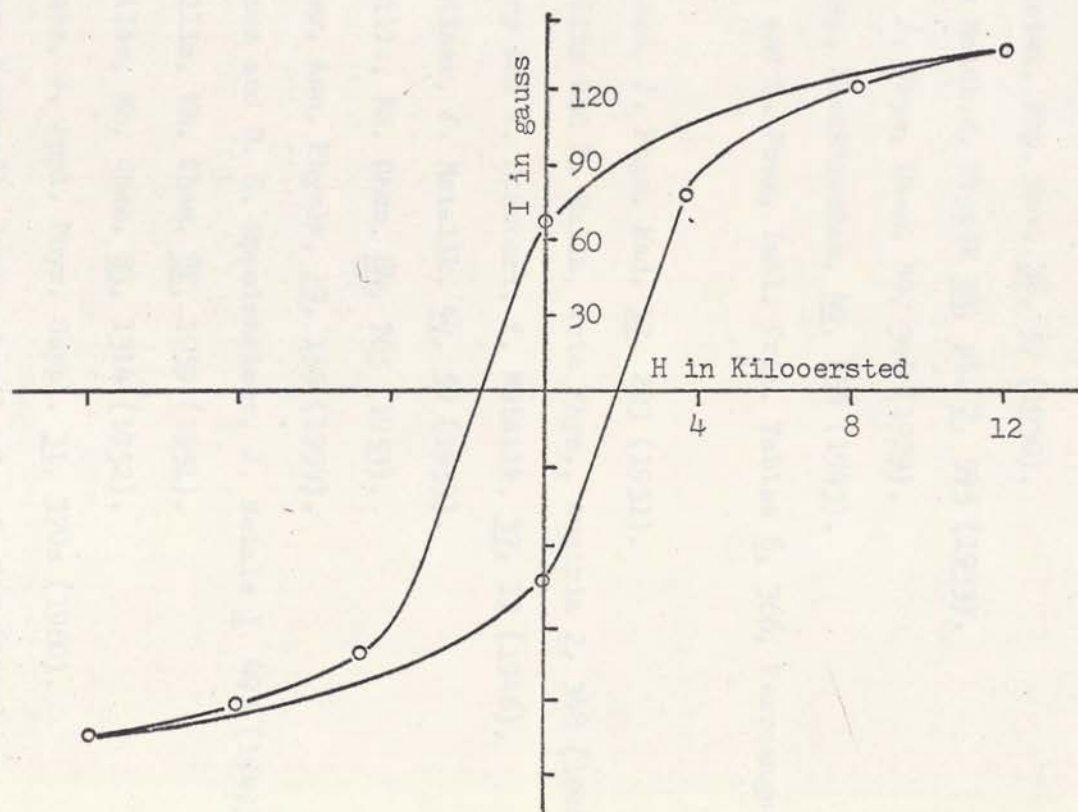


Fig. 21 Hysteresis loop of Ag_5MnSb alloy aged for 200 hours at $140^{\circ}C$

REFERENCES

1. H. H. Potter, *Phil. Mag.* (7) 12, 255 (1931).
2. W. B. Pearson, *A Handbook of Lattice Spacings and Structures of Metals and Alloys.* 125, Pergamon Press (1958).
3. J. C. Slater, *Phy. Rev.* 36, 57 (1930).
4. H. Bethe *Handb.d. Physik* 24, pt. 2, 595 (1933).
5. G. Hagg, *J. Phys. Chem.* B4, 346 (1929).
6. H. Nowotny, *Elecktrochem.* 49, 254 (1943).
7. P. Weiss and G. Foex, *Intl. Crit. Tables* 6, 366, Ferromagnetism, (1929).
8. C. Guillaud, *J. Phys. Rad.* 12, 223 (1951).
9. L. Castelliz and F. Halla, *Acta Phys., Austria* 2, 348 (1948).
10. H. Nowotny and K. Schubert, *f. Metallk.* 37, 17 (1946).
11. S. Valentiner, *f. Metallk.* 44, 59 (1953).
12. L. Castelliz, *Mh. Chem.* 84, 765 (1953).
13. O. Heusler, *Ann. Physik*, 19, 155 (1934).
14. F. A. Hames and D. S. Eppelsheimer, *J. Metals* 1, 495 (1949).
15. L. Castelliz, *Mh. Chem.* 82, 1059 (1951).
16. L. Castelliz, *Mh. Chem.* 83, 1314 (1952).
17. F. A. Hames, *J. Appl. Phys. Suppl.* 31, 370s (1960).
18. F. Heusler, *Verhandl. duet. physik. Ges* 5, 219 (1903).
19. A. J. Bradley and J. W. Rodgers, *Proc. Roy. Soc. (London)* 144A, 340 (1934).

20. Anonymous, Gen. Elec. Rev. 48, 61, Permanent Magnets (1945).
21. A. A. Geisler, Trans. Amer. Soc. Metals, 43, 90 (1951).
22. D. A. Petrow and A. J. Potemkin, Journal of Inorganic Chemistry II, 7 (1957).
23. S. V. Vonsovskij, Ia. s. Shur. M-L (1948).
24. E. I. Kondwiskij, Zhetf, 7, 1117 (1937).
25. E. O. Hall, Philosophical Magazine 4, 730 (1959).
26. W. Bollman, Physical Rev. 103, 1588 (1956).
27. J. A. Hugo and V. A. Phillips, British Journal of Applied Physics 40, 202 (1963).
28. R. C. Glen and J. C. Raley, ASTM Special Technical Publication 339, 60 (1962).
29. A. Fukami, Revue Universelle des Mines, T.XII, 476 (1958).
30. W. C. Elmore, Phy. Rev. 51, 982 (1937).
31. H. Kono, Journal of Physical Society of Japan 13, 12, 1444 (1958).
32. A.J. J. Koch, P. Hokkeling, M.G. V.D. Steeg and K. J. deVos, Journal of Applied Physics, Supplement to 31, 5, 75S (1960).
33. C. S. Barrett, Structure of Metals, Appendix IX, 646, McGraw-Hill Book Company Inc. (1952).
34. A. J. Bradley and P. Jones, Phil. Mag. XII, 1137 (1931).
35. E. I. Estrin, Physics of Metals and Metallography (in English), 19, No. 6, 930 (1965).
36. H. O. Dørum, Avs. Norske, Vidensk., Acad. Oslo I Mat., Nat. Kl, Ni 10, 32, (1929).

37. Ichiro Tsuboya and Makoto Sugihara, Short notes in J. Phys. Soc. Japan: 15, 1534 (1960); 16, 571 (1961); 16, 1257 (1961); 17, 410 (1962); 18, 143 (1963); 20, 170 (1965).
38. Ichiro Tsuboya and Makoto Sugihara, J. Phys. Soc. Japan, 16/10, 1875 (1961); 17, Supplement B-1, 172 (1962).
39. R. F. Mehl and C. S. Barrett, Trans. Amer. Inst. Min. (Metall.) Engrs. 23, 78 (1931).

